

NASA Contractor Report 187488

ICASE INTERIM REPORT 15

FILTERING ANALYSIS OF A DIRECT NUMERICAL SIMULATION
OF THE TURBULENT RAYLEIGH-BENARD PROBLEM

T. M. Eidson
T. A. Zang

NASA Contract No. NAS1-18605
December 1990

DTIC
ELECTE
MAR 21 1991
S E D

INSTITUTE FOR COMPUTER APPLICATIONS IN SCIENCE AND ENGINEERING
NASA Langley Research Center, Hampton, Virginia 23665

Operated by the Universities Space Research Association

NASA

National Aeronautics and
Space Administration

Langley Research Center
Hampton, Virginia 23665-5225

DISTRIBUTION STATEMENT A


Approved for public release;
Distribution Unlimited

97 8 12 104

AD-A232 864

ICASE INTERIM REPORTS

ICASE has introduced a new report series to be called ICASE Interim Reports. The series will complement the more familiar blue ICASE reports that have been distributed for many years. The blue reports are intended as preprints of research that has been submitted for publication in either refereed journals or conference proceedings. In general, the green Interim Report will not be submitted for publication, at least not in its printed form. It will be used for research that has reached a certain level of maturity but needs additional refinement, for technical reviews or position statements, for bibliographies, and for computer software. The Interim Reports will receive the same distribution as the ICASE Reports. They will be available upon request in the future, and they may be referenced in other publications.

Accession For	
NTIS GRA&I	<input checked="" type="checkbox"/>
DTIC TAB	<input checked="" type="checkbox"/>
Unannounced	<input type="checkbox"/>
Justification	
By _____	
Distribution/	
Availability Codes	
Dist	Avail and/or Special
A-1	

Robert G. Voigt
Director



FILTERING ANALYSIS OF A DIRECT NUMERICAL SIMULATION OF THE TURBULENT RAYLEIGH-BENARD PROBLEM

T. M. Eidson¹

M. Y. Hussaini¹

T. A. Zang

ABSTRACT

A filtering analysis of a turbulent flow has been developed which provides details of the path of the kinetic energy of the flow from its creation via thermal production to its dissipation. A low-pass spatial filter is used to split the velocity and the temperature field into a filtered component (composed mainly of scales larger than a specific size, nominally the filter width) and a fluctuation component (scales smaller than a specific size). Variables derived from these fields can fall into one of the above two ranges or be composed of a mixture of scales dominated by scales near the specific size. The filter is used to split the kinetic energy equation into three equations corresponding to the three scale ranges described above.

The data from a direct simulation of the Rayleigh-Benard problem for conditions where the flow is turbulent is used to calculate the individual terms in the three kinetic energy equations. This is done for a range of filter widths. These results are used to study the spatial location and the scale range of the thermal energy production, the cascading of kinetic energy, the diffusion of kinetic energy and the energy dissipation. These results are used also to evaluate two subgrid models typically used in large-eddy simulations of turbulence. Subgrid models attempt to model the energy below the filter width that is removed by a low-pass filter.

¹Research was supported by the National Aeronautics and Space Administration under NASA Contract No. NAS1-18605 while the authors were in residence at the Institute for Computer Applications in Science and Engineering (ICASE), NASA Langley Research Center, Hampton, VA 23665.

1 Introduction

The numerical simulation of turbulent flows has provided considerable insight into flow physics over the last 20 years[13, 14]. The Rayleigh-Benard problem is an example of a specific flow which is better understood because of numerical experiments[7]. The high cost of direct numerical simulations (DNS) and the lack of confidence in extrapolating subgrid models in large-eddy simulations (LES) to new flows has prevented this technology from being more widely used.

A DNS of a turbulent Rayleigh-Benard flow was computed [8] to provide a database for a more extensive analysis of a turbulent flow. The specifics of the simulation and some preliminary data analysis have been presented previously[8]. The focus of the analysis presented in this paper is to use low-bandpass filtering to study the flow field generated by a direct simulation. The intent is to gain insight into the turbulent flow simulated as well as to understand better the filtering and modeling used in large-eddy simulations.

The LES approach is based on splitting the velocity field into a large-scale (filtered velocity) and a small-scale (fluctuation about the filtered velocity) component. The large-scale component is calculated from the appropriately modified Navier-Stokes (and thermal energy) equations (LES equations) and is resolvable. The modification is basically done by adding a subgrid model for the effects of the small-scale motion. A rigorous derivation of the LES equations proceeds by spacially filtering each term in the original equations with a low bandpass filter. Details of the derivation of the LES equations can be found in [14]. The result is a set of differential equations for the filtered variables (usually the velocities and the temperature) with any terms involving a fluctuation variable replaced by an appropriate subgrid model.

To gain insight into the LES approach the total dependent variable fields can be computed using the DNS approach and the terms involving fluctuation quantities in the LES equations calculated to evaluate proposed models. This has been previously done for several flows for which the fluctuation terms (or "turbulent stresses") were directly calculated and compared to models by a correlation analysis, for example [1, 4]. In the present study a correlation analysis similar to those of previous studies is done with the following differences. Since the vertical direction is inhomogeneous, the correlations are only integrated over the horizontal directions. Thus the correlation coefficients are functions of the vertical coordinate. Since the correlation analysis does not compare the mean value of the terms of interest, the horizontal average of these terms are calculated using both a model and the "exact" turbulent stress. These horizontal averages are compared directly to evaluate the model[11]. Also the fine grid data is frequently "smoothed" onto a coarse grid with a grid size approximately equal

to but smaller than the filter widths used. This is not done in this study in order to separate the effect of the numerical method from the effect of the filter width.

While insight into the LES technique is one motivation for this study, the filtering analysis is independent of LES. A range of filter widths from the grid size (or viscous scales, whichever is larger) up to the size of the largest flow scales of the problem can be used to analyze the data from a particular flow simulation. The terms in the various kinetic energy equations based on the filtered and fluctuation velocities can be calculated as functions of the filter width. This yields information similar to that of energy spectra is obtained but with a different perspective.

The filter analysis results presented here are calculated from the output of a DNS of a turbulent Rayleigh-Benard flow (natural convection) at a Rayleigh number (Ra) of 3.8×10^5 and a Prandtl number (Pr) of 0.76. These values were chosen because of the availability of experimental and other simulation data at similar values. Details of the flow, basic variable definitions, and the numerical simulation can be found in Appendix A and in a previous publication [8] where the simulation results were directly compared to other available data, both experimental and numerical[5, 2, 9].

Briefly, the simulation entailed the computation of the 3-dimensional velocity and the temperature fields on a $128 \times 64 \times 64$ grid. The ratio of horizontal to vertical length for the computational volume was 4 and 2 in the x_1 and x_2 directions, respectively. After a steady state flow was developed, data was collected over a time period equal to $10/W_c$, where $W_c = (NuPrRa)^{1/3}$. This period, which should consist of several large eddy turn-over times, was found adequate by Eidson[7]. The average Nusselt number (Nu) calculated from the simulation data is 6.6.

The analysis reported previously [8] shows that the simulation output is well resolved. The global quantities, the Nusselt number and the RMS averages of the velocity and temperature, are in good agreement with the experimental results. The Nu is the closest of several LES and DNS studies to the average of several experimental studies ($Nu = 6.0$). The variation in x_3 (the vertical coordinate) of the various velocity and temperature quantities and the terms of the total kinetic energy equation are in good agreement with the experiments. Most encouraging is the comparison with variance and skewness measurements of the temperature and its vertical derivative by Carroll[2]. While the agreement in magnitude is only fair, the changes in slope with x_3 are excellently predicted. These results along with some consistency checks for the volume averaged terms in the various kinetic energy equations which are made in the current analysis provide a high degree of confidence in the simulation results.

2 Derivation of the Filtered Kinetic Energy Equations

The choice of filter to separate the large-scale and small-scale components is important. The fundamental structures or basis functions of turbulence are not sufficiently understood to select the best filter to separate large-scale from small-scale flow structures. Sharp cut-off filters have been used with some success for LES studies, but they do not allow for flow scales near the filter width to be treated separately from the smaller scales. Consistent with the current understanding of turbulence any smooth low bandpass filter is satisfactory. A Gaussian filter function (shown for 1 dimension) is generally used and thus was selected for this study.

$$\bar{u}(x) = \int_{-\infty}^{\infty} G(x - \bar{x})u(\bar{x})d\bar{x} \quad (1)$$

$$G(x) = \sqrt{\gamma/\pi} \frac{1}{\Delta_f} \exp\left(-\frac{\gamma x^2}{\Delta_f^2}\right)$$

$$\gamma = 6 \quad (2)$$

G is the filter function and Δ_f is the filter width. The above filter is applied only to the two horizontal directions, x_1 and x_2 , to avoid the complications of filtering in an inhomogeneous direction, x_3 . The fluctuating component (denoted by a prime) of a variable, e.g. $u(\vec{x}, t)$, is defined as follows:

$$u'(\vec{x}, t) = u(\vec{x}, t) - \bar{u}(\vec{x}, t) \quad (3)$$

Five filter widths are used to analyze the simulation data—1/16, 1/8, 1/4, 1/2 and 3/4. For comparison, the length of the sides of the control volume for the simulation, L_{x_i} , are:

$$\begin{aligned} L_{x_1} &= 4 \\ L_{x_2} &= 2 \\ L_{x_3} &= 1 \end{aligned} \quad (4)$$

The grid dimensions in the horizontal directions are both 1/32. In the vertical direction a non-uniform Chebyshev grid is used with the average grid size being 1/64.

The derivation of the filtered kinetic energy equations proceeds as follows:

1. The time-dependent partial differential equations for continuity and momentum (Equations 78 and 79 in Appendix A) are filtered term by term.

2. Filtered velocity products are expanded as follows:

$$\begin{aligned}\overline{u_i u_j} &= \overline{\bar{u}_i \bar{u}_j} + \overline{u'_i \bar{u}_j} + \overline{\bar{u}_i u'_j} + \overline{u'_i u'_j} \\ &= M_{ij} + L_{ij} + C_{ij} + R_{ij}\end{aligned}\quad (5)$$

$$R_{ij} \equiv u'_i u'_j \quad (6)$$

$$C_{ij} \equiv u'_i \bar{u}_j + \bar{u}_i u'_j \quad (7)$$

$$M_{ij} \equiv \bar{u}_i \bar{u}_j \quad (8)$$

$$L_{ij} = \overline{M_{ij}} - M_{ij} \quad (9)$$

3. Filtered derivatives of a variable can be shown to be equal to derivatives of the filtered variable.

$$\frac{\partial \bar{u}}{\partial x_i} = \frac{\partial \bar{u}}{\partial x_i} \quad (10)$$

4. Using 2. and 3. to simplify the result of 1., filtered equations are formed.

$$\frac{\partial \bar{u}_i}{\partial x_i} = 0 \quad (11)$$

$$\begin{aligned}\frac{\partial \bar{u}_i}{\partial t} + \frac{\partial M_{ij}}{\partial x_j} &= -\frac{\partial \bar{P}}{\partial x_i} + Pr \frac{\partial \bar{S}_{ij}}{\partial x_j} \\ &\quad - \frac{\partial (C_{ij} + R_{ij} + L_{ij})}{\partial x_j} + Pr Ra T' \delta_{i3}\end{aligned}\quad (12)$$

5. The filtered equations are subtracted from the instantaneous equations to form fluctuation equations.

$$\frac{\partial u'_i}{\partial x_i} = 0 \quad (13)$$

$$\begin{aligned}\frac{\partial u'_i}{\partial t} &= -\frac{\partial P'}{\partial x_i} + Pr \frac{\partial S'_{ij}}{\partial x_j} \\ &\quad + \frac{\partial (C_{ij} - C_{ij})}{\partial x_j} + \frac{\partial (\bar{R}_{ij} - R_{ij})}{\partial x_j} + \frac{\partial \bar{L}_{ij}}{\partial x_j} + Pr Ra T' \delta_{i3}\end{aligned}\quad (14)$$

6. A kinetic energy equation is derived from a dot product of a velocity times the appropriate momentum equation. The total equation is the total velocity times the instantaneous momentum equation. The filtered equation comes from the filtered velocity and the filtered momentum equation and the fluctuation equation uses the appropriate fluctuation quantities. The cross kinetic energy equation is formed as the fluctuation velocity times the filtered momentum equation added to the opposite (filter velocity and fluctuation momentum equation).

• Total Kinetic Energy Equation

$$\begin{aligned}\frac{\partial E}{\partial t} &= -\frac{\partial[u_j(E+P)]}{\partial x_j} + Pr\frac{\partial(u_i S_{ij})}{\partial x_j} \\ &\quad + PrRa(u_3 T) - \frac{1}{2}PrS_{ij}S_{ij} \\ &= D^* + P_T - \epsilon\end{aligned}\tag{15}$$

$$E \equiv \frac{1}{2}u_i u_i\tag{16}$$

$$D^* \equiv -\frac{\partial[u_j(E+P)]}{\partial x_j} + Pr\frac{\partial(u_i S_{ij})}{\partial x_j}\tag{17}$$

$$P_T \equiv PrRa(u_3 T)\tag{18}$$

$$\epsilon \equiv \frac{1}{2}PrS_{ij}S_{ij}\tag{19}$$

• Filtered Kinetic Energy Equation

$$\begin{aligned}\frac{\partial E_F}{\partial t} &= -\frac{\partial[\bar{u}_j(E_F + \bar{P})]}{\partial x_j} + Pr\frac{\partial(\bar{u}_i \bar{S}_{ij})}{\partial x_j} \\ &\quad - \bar{u}_i \frac{\partial(\bar{C}_{ij} + \bar{R}_{ij} + \bar{L}_{ij})}{\partial x_j} + PrRa(\bar{u}_3 \bar{T}) \\ &\quad - \frac{1}{2}Pr\bar{S}_{ij}\bar{S}_{ij} \\ &= D^{*F} + W^F + P_T^F - \epsilon^F \\ &= D^F + P^F + P_T^F - \epsilon^F\end{aligned}\tag{20}$$

$$E_F \equiv \frac{1}{2}\bar{u}_i \bar{u}_i\tag{21}$$

$$D^{*F} \equiv -\frac{\partial[\bar{u}_j(E_F + \bar{P})]}{\partial x_j} + Pr\frac{\partial(\bar{u}_i \bar{S}_{ij})}{\partial x_j}\tag{22}$$

$$D^F \equiv D^{*F} - \frac{\partial \bar{u}_i (\bar{C}_{ij} + \bar{R}_{ij} + \bar{L}_{ij})}{\partial x_j} \quad (23)$$

$$W^F \equiv W_C^{ff} + W_R^{ff} + W_L^{ff} \quad (24)$$

$$P^F \equiv -P_C^{ff} - P_R^{ff} - P_L^{ff} \quad (25)$$

$$P_T^F \equiv Pr Ra' (\bar{u}_3 T) \quad (26)$$

$$\epsilon^F \equiv \frac{1}{2} Pr \bar{S}_{ij} \bar{S}_{ij} \quad (27)$$

• Cross Kinetic Energy Equation

$$\begin{aligned} \frac{\partial E_C}{\partial t} &= -\frac{\partial (u'_j \bar{P} + \bar{u}_j P')}{\partial x_j} + Pr \frac{\partial (u'_i \bar{S}_{ij} + \bar{u}_i S'_{ij})}{\partial x_j} \\ &\quad + \bar{u}_i \frac{\partial (\bar{C}_{ij} - C_{ij})}{\partial x_j} - u'_i \frac{\partial \bar{C}_{ij}}{\partial x_j} \\ &\quad + \bar{u}_i \frac{\partial (\bar{R}_{ij} - R_{ij})}{\partial x_j} - u'_i \frac{\partial \bar{R}_{ij}}{\partial x_j} \\ &\quad + \bar{u}_i \frac{\partial \bar{L}_{ij}}{\partial x_j} - u'_i \frac{\partial \bar{u}_i \bar{u}_j}{\partial x_j} + Pr Ra' (u'_3 T + \bar{u}_3 T') \\ &\quad - Pr \bar{S}_{ij} S'_{ij} \\ &= D^{*C} + W^C + P_T^C - \epsilon^C \\ &= D^C + P^C + P_T^C - \epsilon^C \end{aligned} \quad (28)$$

$$E_C \equiv u'_i \bar{u}_i \quad (29)$$

$$D^{*C} \equiv -\frac{\partial (u'_j \bar{P} + \bar{u}_j P')}{\partial x_j} + Pr \frac{\partial (u'_i \bar{S}_{ij} + \bar{u}_i S'_{ij})}{\partial x_j} \quad (30)$$

$$D^C \equiv D^{*C} + \text{appropriate stress diffusion terms} \quad (31)$$

$$\begin{aligned} W^C &\equiv (W_C^{ft} - W_C^{ff}) + W_C^{pf} + (W_R^{ft} - W_R^{ff}) + W_R^{pf} \\ &\quad + (W_M^{pf} - W_L^{ff}) \end{aligned} \quad (32)$$

$$\begin{aligned} P^C &\equiv -(P_C^{ft} - P_C^{ff}) - P_C^{pf} - (P_R^{ft} - P_R^{ff}) - P_R^{pf} \\ &\quad - (P_M^{pf} - P_L^{ff}) \end{aligned} \quad (33)$$

$$P_T^C \equiv Pr Ra'(u_3' \bar{T} + \bar{u}_3 T') \quad (34)$$

$$\epsilon^C \equiv Pr \bar{S}_{ij} S'_{ij} \quad (35)$$

• Fluctuation Kinetic Energy Equation

$$\begin{aligned} \frac{\partial E_s}{\partial t} &= -\frac{\partial(u_j' P')}{\partial x_j} + Pr \frac{\partial(u_i' S'_{ij})}{\partial x_j} \\ &\quad + u_i' \frac{\partial(\bar{C}_{ij} - C_{ij})}{\partial x_j} + u_i' \frac{\partial(\bar{R}_{ij} - R_{ij})}{\partial x_j} \\ &\quad + u_i' \frac{\partial \bar{L}_{ij}}{\partial x_j} + Pr Ra'(u_3' T') \\ &\quad - \frac{1}{2} Pr S'_{ij} S'_{ij} \\ &= D^{*s} + W^s + P_T^s - \epsilon^s \\ &= D^s + P^s + P_T^s - \epsilon^s \end{aligned} \quad (36)$$

$$E_s \equiv \frac{1}{2} u_i' u_i' \quad (37)$$

$$D^{*s} \equiv -\frac{\partial(u_j' P')}{\partial x_j} + Pr \frac{\partial(u_i' S'_{ij})}{\partial x_j} \quad (38)$$

$$D^s \equiv D^{*s} + \text{appropriate stress diffusion terms} \quad (39)$$

$$W^s \equiv (W_C^{pt} - W_C^{pf}) + (W_R^{pt} - W_R^{pf}) - W_L^{pf} \quad (40)$$

$$P^s \equiv -(P_C^{pt} - P_C^{pf}) - (P_R^{pt} - P_R^{pf}) + P_L^{pf} \quad (41)$$

$$P_T^s \equiv +Pr Ra'(u_3' T') \quad (42)$$

$$\epsilon^s \equiv \frac{1}{2} Pr S'_{ij} S'_{ij} \quad (43)$$

The production terms are composed of the thermal production, P_T and the velocity production, P_z^{ab} . The velocity production takes the following form:

$$P_z^{ab} = -\frac{1}{2} S_{ij}^a Z_{ij}^b, \quad (44)$$

where Z_{ij} is one of the "turbulent stresses" — the Reynolds stress, R_{ij} , the Cross stress, C_{ij} , or the Leonard stress, L_{ij} . Another term which appears in the analysis with a role similar to a stress is M_{ij} . The superscript b refers to the filtered value of the stress ($b = f$) or to the unfiltered or total stress ($b = t$). These terms are called production terms since they have the role of extracting energy from the flow at one velocity scale and adding energy to the flow (or producing energy) at another scale. The term S_{ij}^a is the strain tensor which can be formed from filtered velocities ($a = f$), \bar{S}_{ij} , or from fluctuation (or perturbation) velocities ($a = p$), S'_{ij} . The notation for each of the particular production terms that appear in the set of filtered kinetic energy equations derived in this paper is given in Appendix B.

The production terms are only one form that the work of stresses can take in a kinetic energy equation. Another form is as follows:

$$W_Z^{ab} = -u_i^a \frac{\partial Z_{ij}^b}{\partial x_j} \quad (45)$$

This form will simply be called the work term. The work term can be expanded into the production term plus another work term, T_Z^{ab} which measures the diffusion of the work of the stresses.

$$W_Z^{ab} = T_Z^{ab} - P_Z^{ab} \quad (46)$$

$$T_Z^{ab} = -\frac{\partial(u_i^a Z_{ij}^b)}{\partial x_j} \quad (47)$$

T_Z^{ab} will be referred to as the turbulent stress diffusion. The volume average of the production term is the negative of the volume average of the work term for the same Z and (ab) . Using the straight-forward derivations for the kinetic energy equations described above, the work form naturally appears. Equation 46 can be used to modify pointwise the kinetic energy equations to include the production form. In general, the production form and the work form are not equal locally. One exception is the following:

$$P_R^t = W_R^t \quad (48)$$

Each of the kinetic energy equations can be written as "the time derivative of a kinetic energy equals diffusion terms plus production (or work) terms minus a dissipation term." If the flow has reached a "turbulent steady state" then the time derivative of the kinetic energy averaged over a suitably large spacial region should be zero. The diffusion terms are of the form—the sum of the spacial derivative in each of the 3 directions of a group of terms. The volume average of the diffusion terms can be shown to equal zero for the boundary conditions in this simulation; specifically, periodic boundary conditions in the horizontal directions and zero velocities at the walls. Otherwise, these terms are not zero even for a

horizontal average. The disappearance of the time derivative and diffusion terms for suitable averages partially explains why a "production equals dissipation" assumption is often made in turbulent theories[12, 10]. All the terms in these kinetic energy equation are evaluated in this study.

The filtered momentum and continuity equations become the LES equations after the appropriate terms involving fluctuation variables have been modeled. Actually the fluctuation kinetic energy equations (and even equations for R_{ij} and C_{ij}) with appropriate models can be incorporated into the LES equations, but this has not been generally done[6]. For the present study Equation 15 will be called the total equation since the principal dependent variable, E , is a function of total velocities, u_i . The filtered kinetic energy equation also can be called the resolvable scale equation since the principle variable, E_F , is a function of the filtered velocities, which would be directly resolved in the LES technique. The perturbation kinetic energy equation can be viewed as a subgrid equation since the principle variable, E_S , is a function of velocities with scales below the filter width and for LES, the filter width is of the same order as the grid size. The cross kinetic energy equation can be called the transfer scale equation since it has been suggested that E_C is principally composed of velocity scales that transfer energy from the filtered region to the fluctuation region[1]. Equations 20, 28 and 36 will be referred to as the set of filtered kinetic energy equations.

The total potential energy equation is included for reference. The potential energy equation is derived by multiplying the thermal energy equation by $-PrRa(x_3)$. Note that the term, $PrRa(u_3T_r)$, removes energy (has a negative sign) from the potential energy equation where it adds energy (has a positive sign) to the total kinetic energy equation.

$$\frac{\partial \Phi}{\partial t} + u_j \frac{\partial \Phi}{\partial x_j} = -PrRa(u_3T_r) - PrRa \left(x_3 \frac{\partial^2 T_r}{\partial x_j^2} \right) \quad (49)$$

Φ is the non-dimensional potential energy.²

$$\Phi = -PrRaT_r x_3 \quad (50)$$

²In dimensional form, Φ is defined as follows:

$$\Phi = \frac{(\rho g - \rho_c g)}{\rho_o} = -g\beta T_r x_3$$

3 Data Analysis Details

When the kinetic energy equations are horizontally averaged, the cross kinetic energy equation can be simplified. The simplification is a consequence of the following identity.

$$\begin{aligned}
 \langle f\bar{g} \rangle &= \int_{-\infty}^{\infty} f(x) \left(\int_{-\infty}^{\infty} G(x-x')g(x')dx' \right) dx \\
 &= \int_{-\infty}^{\infty} g(x') \left(\int_{-\infty}^{\infty} G(x-x')f(x)dx \right) dx' \\
 &= \langle \bar{f}g \rangle,
 \end{aligned} \tag{51}$$

where f and g are smooth, continuous functions of x . The $\langle \rangle$ denote a horizontal average. When the above identity is applied to certain production and work terms the following relationships can be derived.

$$\begin{aligned}
 \langle \bar{u}_i \frac{\partial L_{ij}}{\partial x_j} \rangle &= \langle \bar{u}_i \frac{\partial \bar{M}_{ij}}{\partial x_j} - \bar{u}_i \frac{\partial M_{ij}}{\partial x_j} \rangle \\
 &= \langle \bar{u}_i \frac{\partial \bar{M}_{ij}}{\partial x_j} - \bar{u}_i \frac{\partial \bar{M}_{ij}}{\partial x_j} \rangle \\
 &= - \langle u'_i \frac{\partial \bar{M}_{ij}}{\partial x_j} \rangle
 \end{aligned} \tag{52}$$

$$\begin{aligned}
 \langle \bar{u}_i \frac{\partial (R_{ij} - \bar{R}_{ij})}{\partial x_j} \rangle &= \langle \bar{u}_i \frac{\partial R_{ij}}{\partial x_j} - \bar{u}_i \frac{\partial \bar{R}_{ij}}{\partial x_j} \rangle \\
 &= \langle u'_i \frac{\partial \bar{R}_{ij}}{\partial x_j} - \bar{u}_i \frac{\partial \bar{R}_{ij}}{\partial x_j} \rangle \\
 &= \langle u'_i \frac{\partial \bar{R}_{ij}}{\partial x_j} \rangle
 \end{aligned} \tag{53}$$

$$\langle \bar{u}_i \frac{\partial (C_{ij} - \bar{C}_{ij})}{\partial x_j} \rangle = \langle u'_i \frac{\partial \bar{C}_{ij}}{\partial x_j} \rangle \tag{54}$$

$$\langle \bar{S}_{ij} L_{ij} \rangle = - \langle S'_{ij} \bar{M}_{ij} \rangle \tag{55}$$

$$\langle \bar{S}_{ij} (R_{ij} - \bar{R}_{ij}) \rangle = \langle S'_{ij} \bar{R}_{ij} \rangle \tag{56}$$

$$\langle \bar{S}_{ij} (C_{ij} - \bar{C}_{ij}) \rangle = \langle S'_{ij} \bar{C}_{ij} \rangle \tag{57}$$

These relationships can be used to simplify the horizontally averaged cross kinetic energy equation to the following form:

$$\langle \frac{\partial E_C}{\partial t} \rangle = \langle D^*C + 2W_C^{pf} + 2W_R^{pf} + 2W_M^{pf} + P_T^C - \epsilon^C \rangle \tag{58}$$

or

$$\left\langle \frac{\partial E_C}{\partial t} \right\rangle = \left\langle D^C - 2P_C^{\sigma f} - 2P_R^{\sigma f} - 2P_M^{\sigma f} + P_T^C - \epsilon^C \right\rangle \quad (59)$$

Although these equations are derived for continuous arithmetic, the derivation for discrete arithmetic is straight-forward.

The data analysis proceeded as follows:

1. The velocity and temperature values at each grid point were saved for 322 time steps during a "steady state" portion of the DNS. These time steps are equally spaced over a time period of $10/W_c$. For each filter width, the various production, work, diffusion and dissipation terms are calculated at each grid point for a particular time step. All derivatives and multiplications of variables are done in the same manner as the original simulation[8]. The analysis arithmetic is done using 32-bits only compared to 64-bits used in the original simulation.
2. The terms are then horizontally averaged, denoted by $\langle \rangle$, and volume averaged, denote by $\{ \}$. The data was then "long" time averaged over about 80% of the "steady state" portion of the simulation—the time period shown in Figure 1.

In the plots of the horizontal averages versus x_3 , the curves are not always symmetrical about $x_3 = 0$, particularly the production/work terms (e.g. Figure 16). Specifically, some of the variations with x_3 (or "humps") appear to be too irregular to be a "general steady state" solution that would be found regardless of initial conditions (and possibly small changes in boundary conditions such as the aspect ratio of the computational volume). The horizontal and volume averages of the velocities should tend to zero since viscosity should dissipate any mean horizontal motion. "Non-symmetric or non-zero" initial conditions or a weak organized flow caused by an instability may persist for a long period of time[3]. Plots of the horizontal velocity averages showed that a small patterned flow did exist during the entire simulation. In Figure 1a, $\{u_1\}$ and $\{u_2\}$ are small compared to the RMS levels in Figure 1b but show no tendency to dissipate. A change in the pattern of $\{u_i\}$ was observed in Figure 1b between the first and second half of the simulation. Differences in $\langle u_i \rangle$ versus x_3 between the two halves are also observed. The pattern in Figure 2a for 4 selected time steps is observed during the entire simulation with the peaks oscillating several times from positive to negative. This pattern could have resulted from a large cellular motion that filled the entire vertical region. The pattern in Figure 2b is observed from the middle to the end of the simulation. This form could result from cellular motion of about half the size of the distance between the plates. $\langle u_3 \rangle$ is several orders of magnitude smaller than $\langle u_1 \rangle$ and $\langle u_2 \rangle$ due to

the effect of the continuity equation and the periodic boundary conditions in the horizontal directions. These facts lead one to suspect that the component of the flow causing the non-zero magnitude of $\langle u_1 \rangle$ and $\langle u_2 \rangle$ is related to the irregular "humps" in the velocity production terms. $\langle u_1 \rangle$ and $\langle u_2 \rangle$ are a maximum of about 20 at each time step. The production terms are proportional to velocity cubed and the "humps" are generally of order $20^3 = 8000$. Also the x_3 size of the "humps" is consistent with the variations in x_3 seen in Figure 2b as well as similar plots at other time steps (not shown).

One other source of inaccuracy that is investigated is the effect of aliasing. Although there is no apparent aliasing problems in the simulation, several of the operations in this analysis—multiplication, taking derivatives, extracting perturbation variables—increase the relative size of the higher wavenumber components of the field being calculated. As a check, the original velocity fields were expanded by spectral methods onto a grid with twice the resolution and a limited set of results were calculated on this grid. Although some differences in the results are observed locally (a small 3-dimensional spacial region at one time step) for the most sensitive quantities being calculated, no significant difference is found between the horizontal averages calculated on the original grid and on the expanded grid.

4 Volume Averages

The data calculated for the five filter widths specified previously are discussed below where the terms of the kinetic energy equations have been averaged over the computation control volume. The filter widths, listed in Table 1, can be compared to the size of the control volume for reference, which is 1(height) by 4 by 2 in units of non-dimensional length. The data is long time averaged.

In Table 1 the non-zero volume averages for the terms in Equations 20, 28 and 36 along with the kinetic energy associated with each equation are shown. Also the values for the diffusion terms, which should give zero, are included as a measure of the numerical accuracy of the original simulation and current analysis. In Table 2 the fraction of kinetic energy in the scales below the filter width is given.

These volume averages are plotted versus filter width in Figures 3a-d. For the small filter widths the filtered kinetic energy (and terms in the associated equation) dominates with the cross kinetic energy (and terms) being larger than the fluctuation equivalent. At the larger filter widths, the energy is more evenly divided. In each of the 3 kinetic energy equations the thermal production and the dissipation terms dominate and almost balance each other. The other non-zero volume averages, the production/work terms, are smaller.

The production of the fluctuating flow is assumed generally to be due to thermal effects

	E	D^*	P_T	ϵ	P^F
	8848	3264	1639152	1630896	0
filter width	E_F	D^{*F}	P_T^F	ϵ^F	P^F
1/16	8712	3216	1605264	1559800	-37386
1/8	8351	3088	1520776	1403512	-109760
1/4	7326	2704	1302627	1080189	-216349
1/2	5261	1936	916234	657181	-254166
3/4	3629	1280	632675	418080	-209019
	E_C	D^{*C}	P_T^C	ϵ^C	P^C
1/16	135	48	32961	67605	34498
1/8	466	160	107777	193472	85342
1/4	1254	480	260544	364362	102924
1/2	2333	912	424360	429592	2853
3/4	2819	1072	488818	406334	-86228
	E_S	D^{*S}	P_T^S	ϵ^S	P^S
1/16	3	0	929	3494	2540
1/8	33	16	10600	33913	23207
1/4	270	80	75983	186347	110073
1/2	1255	448	298560	544125	244862
3/4	2401	896	517659	806482	287344

Table 1: Volume Averaged Kinetic Energy Equation Terms

filter width	$\frac{(E_C + E_S)}{(E_F + E_C + E_S)}$
1/16	0.015
1/8	0.056
1/4	0.172
1/2	0.405
3/4	0.590

Table 2: Fraction of kinetic energy below the filter width.

for the large-scale motion and due to the velocity cascading mechanism for the generation of intermediate and small-scale motion. The results of the current simulation are able to quantify this notion at least for one Ra. The thermal production occurs at scales larger than $1/8$ based on the observation that $P_T^S + P_T^C$, the thermal production below the filter width, is reduced to 7% of the total dissipation at this filter width. At the largest filter width, the equivalent value is 60%. Thus the thermal production, while concentrated at the largest scales, is spread over a significant range.

The velocity production or cascading energy is shown in Figure 3c. As the filter width increases, the velocity production terms in each of the 3 kinetic energy equations must approach zero. Assuming that these terms have reached their maximum value near the largest filter used in this study, only about 20% of the total dissipation (based on P^S at $\Delta_f = 3/4$) is involved in the cascading mechanism.

In Figures 4 and 5 simple schematics of the energy flows are presented. The conversion of energy from one type to another occurs over a range of flow scales and is not generally local to a specific spacial region. (The effects of a core and boundary-layer region are not distinguished in this volume average analysis.) The average transfer of energy from the filtered to the cross to the fluctuation equation is done by the velocity production/work terms. For the flow simulated in this study, energy on the average is extracted from the filtered equation and added to the fluctuation equation. The cross velocity production was either positive or negative depending on the filter width.

5 Horizontal Averages

In this section the variation with x_3 of the horizontal averages of the terms of the set of filtered kinetic energy equations (Equations 20, 28 and 36) are examined. Plots of the terms in the total kinetic energy equation (Equation 15 and Figure 6a) and the total potential energy equation (Equation 49 and Figure 6b) are included for reference.

The first observation is the existence of boundary-layer regions near the wall where the various terms have significantly different behavior from the center layer. In a previous analysis of this simulation data, a boundary-layer region of thickness 0.23 next to each wall was determined[8]. This agreed with experimental data, in particular that of Carroll[2]. All of the terms studied in this analysis exhibited a region, significantly different in character from the core region, near the walls with approximately this thickness. (Figures 7 to 9) In the core region most of the kinetic energy equation terms are relatively constant with the major exceptions being the production/work terms. The production/work terms are generally smaller in magnitude than the other terms in the same equation with the same filter

width. Their variations with x_3 could be due to the low frequency, patterned flow mentioned previously that persisted throughout the simulation. In the boundary layer almost all the terms are significant and exhibit large variations in x_3 . The production terms approach zero as they near the walls while the dissipation and diffusion terms (due to the viscous component, see below) approach a maximum value at the wall.

The total diffusion, D , in each of the three equations has a similar variation with x_3 (Figure 7). The diffusion is transferring energy from the core to the boundary layer. The diffusion in the filtered equation increases as Δ_f is decreased. However, as Δ_f is decreased, the diffusion in the fluctuation equation becomes smaller until it is negligible. The diffusion in the cross equation is larger than that in the fluctuating equation but also decreases with decreasing Δ_f . The diffusion is composed of the stress diffusion plus the two component of D^* —the pressure component (pressure plus kinetic energy in the filtered equation) and the viscous component. Both contribute mainly near the wall, although the pressure component has a significant core contribution in some cases. Figures 8a and 8b are examples of the typical variation with x_3 of these terms, which are similar to the same terms in the total kinetic energy equation (Figure 6a). The stress diffusion (Figure 8c) has a shape similar to the pressure component and is generally the smallest of the diffusion components.

An example of the dissipation terms is shown in Figure 9a. There was little difference in the shape of the dissipation versus x_3 for the different equations and filter widths. The thermal production terms also exhibited this consistency of shape. An example is shown in Figure 9b. The magnitudes of these terms for different Δ_f can be inferred from Figures 3b and 3a. One other quantity of interest is the kinetic energy itself. The variation with x_3 of the three kinetic energies was similar although the fluctuation kinetic energy did not exhibit the peak in magnitude in the boundary layer as did the other two (Figures 9c and 3d). All three showed no significant variation in shape with Δ_f . The variation with time of the kinetic energies can be inferred from Figure 1b.

6 Kinetic Energy Equations

All the terms of the filtered kinetic energy equation are plotted together in Figure 10 for 3 filter widths. The dissipation, ϵ , is positive when it extracts energy, which is opposite to the other terms—due to writing $-\epsilon$ for the dissipation in the kinetic energy equations. The terms have similar variations in x_3 to those of the terms in the total kinetic energy equation (Figure 6a), except that the velocity production terms are non-zero although they are small. The volume averages for these same terms except for the diffusion which is zero are plotted versus Δ_f in Figures 11a and 11b. While the thermal production balances the dissipation

globally (volume averaged), this is not true locally (horizontally averaged), particularly in the core. For small Δ_f the dissipation in the core increases but still does not balance the production.

For a large Δ_f , the filtered equation describes the energy flow of the large scales. From Figures 12a and 12b the energy extracted from the large-scale flow by the production terms is mainly in the boundary layer. For the smaller Δ_f in Figure 12c the fluctuations due to the scales smaller than the filter width are extracting energy more uniformly across the entire fluid layer. Another observation is the change in importance of the three production terms shown in Figure 11b. At small Δ_f , P_C^{ff} and P_L^{ff} are dominant. At the larger Δ_f where C_{ij} and L_{ij} approach zero, P_R^{ff} becomes largest—although this term also must approach zero for very large Δ_f .

The cross kinetic energy equation, Equation 28, contains 9 production/work terms. For horizontal and volume averages, a simplified form reduces the number of terms to 3 (Equation 59). Since no particular physical significance can be associated with either form, the data will be plotted for the reduced form for simplicity.

The cross kinetic energy equation terms are shown in Figures 13 and 14. For larger Δ_f , the variation of the terms with x_3 is similar to that in the filtered equation (Figure 10). One difference is that the dissipation is more significant in the core for the cross equation than for the filtered equation. For smaller Δ_f , the velocity production is almost equal to the thermal production; whereas, in the filtered equation the thermal production dominates the velocity production for all Δ_f . This is due to the large magnitude of the velocity production component, P_M^{pf} .

Similar plots for the terms in the fluctuation kinetic energy equation are shown in Figures 15 to 17. To simplify the plots, the two velocity production terms involving C_{ij} have been added together. The same was done with the R_{ij} terms. In each case, one of the two terms is significantly smaller.

$$P_C^{pt} \gg P_C^{pf} \quad (60)$$

$$P_R^{pt} \ll P_R^{pf} \quad (61)$$

The data for the fluctuation equation is similar to that for the cross and filtered equation. However, the boundary layer and core regions are not as well defined as in the other two equations. On close inspection there appears to be a region in the core merging with the boundary layer— $0.2 < |x_3| < 0.4$ —where the velocity production and the diffusion have increased importance. Another difference from the other two equations is that the thermal production does not approximately balance dissipation even on a volume averaged basis. The velocity production is even slightly larger than the thermal production for small Δ_f .

The magnitude of P^S is not mainly due to one component, as for the cross equation, but the "L, C and R" components vary in importance as a function of Δ_f (Figure 17b).

7 Subgrid Scale Modeling

Calculation of the terms in the kinetic energy equation using the direct simulation data can be used to study subgrid models for LES. For example, the production terms for $\bar{R}_{ij} + \bar{C}_{ij}$ can be calculated directly (referred to as "exact") and compared to the same term calculated with a model for $\bar{R}_{ij} + \bar{C}_{ij}$. The "exact" and modeled production terms can then be compared using a correlation analysis[1, 4]. However, a direct comparison of some average of the production terms (such as an average over homogeneous directions) can be used also to evaluate the models. Since the selection of models and model constants is often based on the correct prediction of energy transfer between different flow scales in many LES studies [1], the correct prediction of the magnitudes of the production terms should be an important model criterion. In particular, $P_{R+C}^{ff} \equiv P_R^{ff} + P_C^{ff}$, which extracts energy from the filtered flow field (Equation 20), should provide the most important criterion. The analysis in this study is only the first step in evaluating subgrid models. Conclusions drawn from this analysis of DNS data which suggest changes in subgrid modeling must be verified in an actual LES.

The main thrust of this study was to evaluate the behavior of commonly used subgrid models for natural convection flows. To the authors knowledge, most studies of subgrid modeling using DNS data have been done using isothermal flows. The model comparisons were made using a range of filter widths from 0.0625 to 0.75 . These filter widths were chosen so that the split of kinetic energy between the filtered velocity field and the subgrid velocity field would include the range found in typical LES studies. The Smagorinsky model and the scale-similarity model were the models tested since these are the two most frequently used models. The Smagorinsky model is [7]:

$$\overline{u_i' u_j'} - \frac{1}{3} \delta_{ij} \overline{u_k' u_k'} = -K \bar{S}_{ij} \quad (62)$$

$$K = \frac{(C_K \Delta_S)^2}{\sqrt{2}} \bar{S}$$

$$\bar{S} = (\bar{S}_{ij} \bar{S}_{ij})^{\frac{1}{2}}$$

$$\Delta_S = \text{minimum } (\Delta_f \text{ or distance to nearest wall})$$

$$C_K = \text{model constant} \quad (63)$$

The scale-similarity model is [1]:

filter width	C_K
1/16	0.047
1/8	0.055
1/4	0.069
1/2	0.114
3/4	0.175

Table 3: Smagorinsky model constant, C_K , adjusted so that the model predicts the "exact" value of P_{R+C}^{ff} at each filter width.

$$\overline{u_i' u_j'} - \frac{1}{3} \delta_{ij} \overline{u_k' u_k'} = (\bar{u}_i \bar{u}_j - \bar{u}_i \bar{u}_j) - \frac{1}{3} \delta_{ij} (\bar{u}_n \bar{u}_n - \bar{u}_n \bar{u}_n) \quad (64)$$

The value of C_K for the Smagorinsky model is one of the results of the current analysis. Generally, $C_K = 0.21$ has been used in natural convection simulations [7], but this value assumes that the grid size, Δ , is used as the length scale, Δ_s . Studies for homogeneous turbulence have shown that C_K should be reduced by a factor of 2 or 3 when Δ_f is used instead. Therefore, a value between 0.07 to 0.14 should be assumed as a target value of C_K . If the constant of the Smagorinsky model is adjusted to match the same volume-averaged production as the "exact" term, the value of C_K varies as shown in Table 3. The Smagorinsky constant can also be allowed to vary with x_3 . If C_K is adjusted at each x_3 to give the simulation results, the modified C_K varies with x_3 as shown in Figure 18. A value of 0.05 gives best agreement in the center region and the value of C_K varies significantly closer to the walls. C_K in the side regions increases with filter width.

$\langle P_{R+C}^{ff} \rangle$ is plotted in Figure 19 for the simulation data (labeled "exact") and for the two models mentioned above. $\langle P_{R+C}^{ff} \rangle$ for the Smagorinsky model was calculated at the different filter widths with the value of C_K in Table 3. Since the scale similarity model has no adjustable constant, $\{P_{R+C}^{ff}\}$ calculated using this model is different from the other two in the horizontal average plots. $\{P_{R+C}^{ff}\}$ versus filter width is plotted in Figure 20 where the same value of C_K (0.07) was used for all filter widths. The data in Figure 19 gives a more local comparison of the models to the "exact". At the small filter widths, the scale-similarity model gives good agreement with the "exact" value as x_3 (the inhomogeneous direction) is varied. For larger filter widths, the agreement is not as good and the scale similarity model even predicts negative values for $\langle P_{R+C}^{ff} \rangle$ in the core region while the "exact" value remains positive. The Smagorinsky model shows no agreement with the variation of spacial distance in an inhomogeneous direction and can only be providing a global agreement in

filter width Smagorinsky scale-similarity

1/16	0.07	0.99
1/8	0.12	0.97
1/4	0.19	0.89
1/2	0.19	0.74
3/4	0.14	0.68

Table 4: Volume average of the correlation of P_{R+C}^{ff} calculated directly with P_{R+C}^{ff} calculated using a model for \bar{R}_{ij} and \bar{C}_{ij} .

energy dissipation as has generally been believed. For comparison of these results with other calculations, the fraction of energy below the filter width shown in Table 2 may be a better parameter than the value of the filter width itself.

Previous studies have estimated that the scale-similarity model has a very small contribution to the subgrid turbulent production and dissipation [1]. The current results show that the fraction of the “exact” production energy predicted by the scale-similarity model varies significantly with Δ_f (Figure 20). For the smallest Δ_f tested (too small to be of use in a LES), the scale-similarity model prediction of $\langle P_{R+C}^{ff} \rangle$ is almost equal to the “exact” value (Figure 19). As Δ_f increases, this fraction predicted decreases to 12% for $\Delta_f = 0.75$. As mentioned above, the value of C_K that best matches $\{P_{R+C}^{ff}\}$ of the Smagorinsky model to the “exact” value also varies with Δ_f . In most LES studies the selection of a model and the model constants is reported without reference to the fraction of energy in the subgrid field. Based on these results it appears that the choice of models and model constants should be a function of the energy fraction in the subgrid field.

The correlations of the two models with the “exact” term based on the simulation data for $\langle P_{R+C}^{ff} \rangle$ are shown in Figure 21. The horizontal correlations are formed as follows:

$$corr(x_3) = \frac{\langle (a - \langle a \rangle)(b - \langle b \rangle) \rangle}{\sqrt{\langle (a - \langle a \rangle)^2 \rangle} \sqrt{\langle (b - \langle b \rangle)^2 \rangle}} \quad (65)$$

where a and b are functions of x_1 , x_2 and x_3 . The correlations of P_{R+C}^{ff} and W_{R+C}^{ff} (not shown) have roughly the same magnitudes. The correlation of W_{R+C}^{ff} is the same “scalar level” comparison in the study done by Bardina et. al.[1], except that the correlations were done in horizontal planes in the present study. The vertical average of the results in Figure 21 are shown in Table 4. The correlation levels in the current study show a significantly higher correlation for the scale-similarity model than for the Smagorinsky model, similar to that in

[1]. In [1] the correlation coefficients were 0.50 and 0.58 for the scale similarity model and 0.36 and 0.05 for the Smagorinsky model. The flows used in that study were homogenous isotropic turbulence and homogenous shear turbulence. The current correlation results are in general agreement with [1]. The scale similarity model gives better local agreement with the "exact" results than the Smagorinsky model.

8 Concluding Remarks

A formal study of the set of kinetic energy equations derived from filtering the original momentum equations has provided insight into the physics of the current flow. In particular, the variation of the thermal and velocity production terms with scale (or Δ_f) has been quantified. When one deals with the large quantity of detailed data that exist in turbulent flows some averaging of the details is necessary to study the flow. Fourier spectral analysis provides information on the spacially averaged energy flow. The filter analysis presented here provides similar information but with a spacially local average. Also, the current study has shown that the diffusion terms are not negligible, especially near the walls. The Smagorinsky models assumes production equals dissipation, neglecting diffusion.

The extension of the calculation of the terms of the filtered set of kinetic energy equations to evaluate subgrid models is natural. One difference in this study from previous "a priori" studies is that the fine scale calculations of the direct simulation were not projected onto a coarse grid before calculating the model results. This was done to decouple the effect of the subgrid filtering from the filtering that results from projecting onto a coarse grid.

The validity of the "a priori" studies to investigate LES models using DNS data is an open issue. Possibly the approach taken in this study when applied to a wider range of flows and then compared in actual LES studies can help clarify the process of determining subgrid models. In particular, a better understanding of the effect of combining the Smagorinsky model with the scale similarity model (called the linear combination model) is needed. In the study where the linear combination model was proposed [1], it was suggested that the scale similarity part contributed little (about 5%) to the energy dissipation. The current results suggest that the amount varies with Δ_f and is generally a larger percentage.

9 Appendix A - The Rayleigh-Benard problem

The Rayleigh-Benard problem is a simple geometry, laboratory-type problem used to study natural convection. The problem entails the study of the fluid motion and thermal convection of a rectangular fluid layer which is typically heated from below. The layer is typically

thin, has no mean pressure gradient in the horizontal directions, and has uniform boundary conditions in the horizontal directions.

Wall boundary conditions are assumed at the upper and lower fluid edges. Periodic boundary conditions are assumed in the horizontal directions. The vertical coordinate, x_3 , was defined as zero halfway between the two walls for this study.

1. Variables:

- fluid properties (all constant) -
 - ν kinematic viscosity
 - α thermal diffusivity
 - β coefficient of thermal expansion
 - ρ_o reference fluid density
 - g acceleration of gravity
- geometry constants -
 - h distance between the two horizontal walls
- dependent variables -
 - u_i fluid velocity, $i = 1, 2, 3$
 - T_a fluid temperature
 - P_a fluid pressure
 - ρ fluid density
- independent variables -
 - x_i spacial coordinates, $i = 1, 2, 3$
 - t time
- flow constants -
 - T_o temperature at lower wall
 - ΔT temperature difference between upper and lower wall

2. Boundary conditions:

$$\begin{aligned} u_i &= 0 & x_3 &= \pm h/2 \\ T_a &= T_o & x_3 &= -h/2 \\ T_a &= T_o - \Delta T & x_3 &= h/2 \\ \Delta T &> 0 \end{aligned}$$

3. Boussinesq assumption:

$$\rho g = \rho_o g - \rho_o g \beta (T_a - T_o) \quad (66)$$

4. Removal of static temperature and pressure gradient

$$T_a(\vec{x}, t) = T_r(\vec{x}, t) + T_o \quad (67)$$

$$T_r(\vec{x}, t) = T(\vec{x}, t) - \frac{\Delta T}{2h}(x_3 + h) \quad (68)$$

$$-\frac{\partial P_s}{\partial x_i} = -\frac{\partial P}{\partial x_i} + X_i^P, \quad i = 1, 2 \quad (69)$$

$$-\frac{\partial P_s}{\partial x_3} = -\frac{\partial P}{\partial x_3} + \rho_o g \left(1 + \beta \frac{\Delta T}{2h}(x_3 + h) \right) \quad (70)$$

5. Non-dimensionalize by α , ΔT , ρ_o and h

$$\hat{u}_i \equiv \frac{u_i}{\alpha/h} \quad (71)$$

$$\hat{P} \equiv \frac{P}{\rho_o \alpha^2 / h^2} \quad (72)$$

$$\hat{T} \equiv \frac{T}{\Delta T} \quad (73)$$

$$Ra \equiv \frac{g \beta \Delta T h^3}{\nu \alpha} \quad (74)$$

$$Pr \equiv \frac{\nu}{\alpha} \quad (75)$$

$$\hat{x}_i \equiv \frac{x_i}{h} \quad (76)$$

$$\hat{t} \equiv \frac{t}{h^2/\alpha} \quad (77)$$

6. Governing Equations

$$\frac{\partial \hat{u}_i}{\partial \hat{x}_i} = 0 \quad (78)$$

$$\frac{\partial \hat{u}_i}{\partial \hat{t}} + \hat{u}_j \frac{\partial \hat{u}_i}{\partial \hat{x}_j} = -\frac{\partial \hat{P}}{\partial \hat{x}_i} + Pr \frac{\partial \hat{S}_{ij}}{\partial \hat{x}_j} + Pr Ra T \delta_{i3} \quad (79)$$

$$\frac{\partial \hat{T}}{\partial \hat{t}} + \hat{u}_j \frac{\partial \hat{T}}{\partial \hat{x}_j} = \frac{\partial^2 \hat{T}}{\partial \hat{x}_j^2} + \hat{u}_3 \quad (80)$$

$$\hat{S}_{ij} = \frac{\partial \hat{u}_i}{\partial \hat{x}_j} + \frac{\partial \hat{u}_j}{\partial \hat{x}_i} \quad (81)$$

In the main body of this paper the non-dimensional variables and equations will be used. The $\hat{}$ notation will be removed for convenience.

10 Appendix B - Production Terms

$$P_C^{ft} \equiv -\frac{1}{2} \overline{S}_{ij} C_{ij} \quad (82)$$

$$P_C^{ff} \equiv -\frac{1}{2} \overline{S}_{ij} \overline{C}_{ij} \quad (83)$$

$$P_C^{st} \equiv -\frac{1}{2} S'_{ij} C_{ij} \quad (84)$$

$$P_C^{sf} \equiv -\frac{1}{2} S'_{ij} \overline{C}_{ij} \quad (85)$$

$$P_R^{ft} \equiv -\frac{1}{2} \overline{S}_{ij} R_{ij} \quad (86)$$

$$P_R^{ff} \equiv -\frac{1}{2} \overline{S}_{ij} \overline{R}_{ij} \quad (87)$$

$$P_R^{st} \equiv -\frac{1}{2} S'_{ij} R_{ij} \quad (88)$$

$$P_R^{sf} \equiv -\frac{1}{2} S'_{ij} \overline{R}_{ij} \quad (89)$$

$$P_L^{ft} \equiv -\frac{1}{2} \overline{S}_{ij} L_{ij} \quad (90)$$

$$P_L^{ff} \equiv -\frac{1}{2} \overline{S}_{ij} \overline{L}_{ij} \quad (91)$$

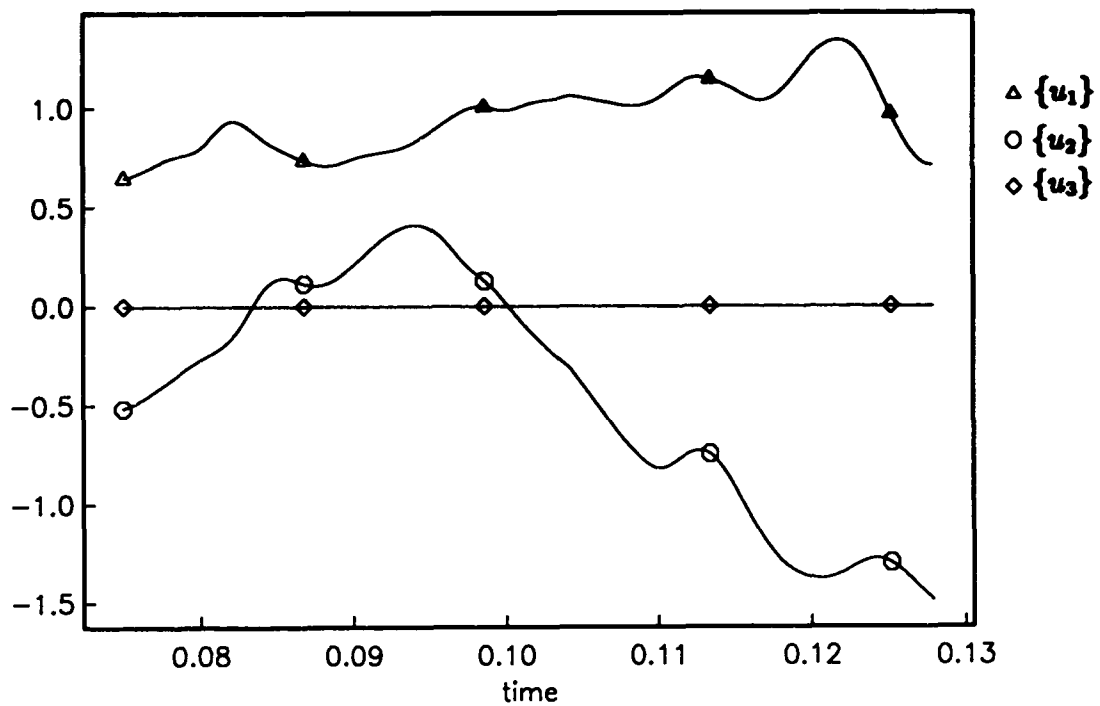
$$P_M^{st} \equiv -\frac{1}{2} S'_{ij} (\overline{u}_i \overline{u}_j) \quad (92)$$

$$P_M^{sf} \equiv -\frac{1}{2} S'_{ij} (\overline{u}_i \overline{u}_j) \quad (93)$$

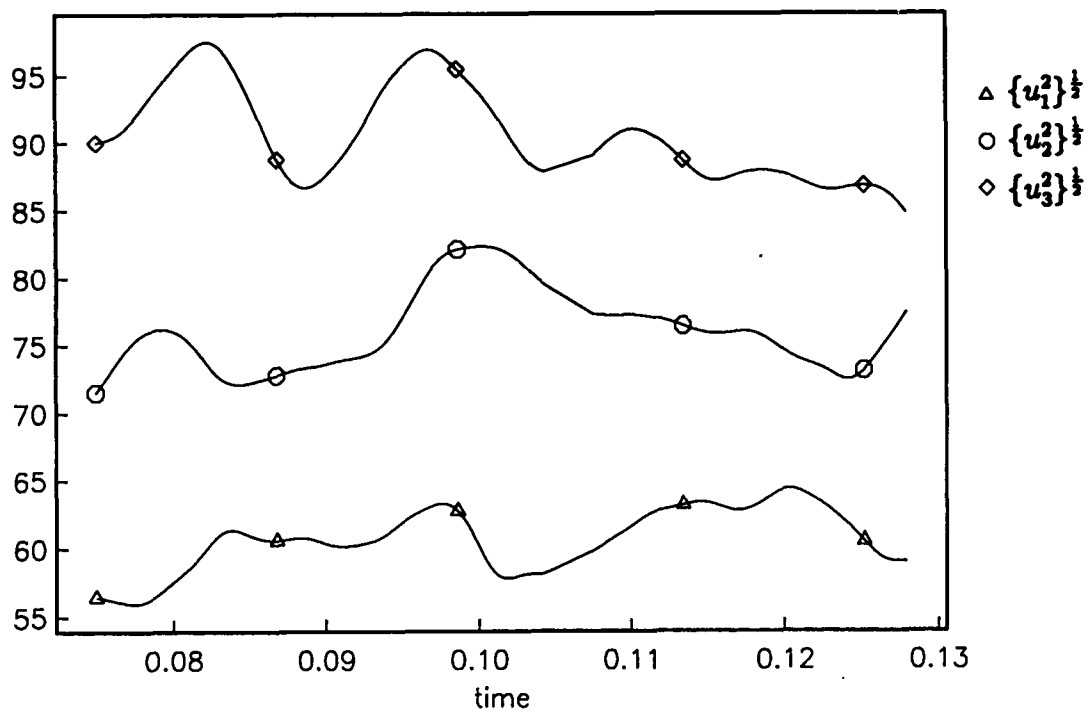
References

- [1] Bardina, J., Ferziger, J.H. and Reynolds, W.C., 1983, Improved turbulence models based on large eddy simulation of homogeneous, incompressible, turbulent flows, *Report No. TF-19*, Dept. of Mech. Engr., Stanford University.
- [2] Carroll, J.J., 1976, The thermal structure of turbulent convection. *J. Atmos. Sc.* **33**, 642.
- [3] Busse, F.H., 1985, Transition to turbulence in Rayleigh- Benard Convection. *Topics in Applied Physics: Hydrodynamic Instabilities and the Transition to Turbulence* **45**, ed. H.L. Swinney and J.P. Gollub, Springer-Verlag.
- [4] Clark, R.A., Ferziger, J.H. and Reynolds, W.C., 1979, Evaluation of subgrid-scale turbulence models using a fully simulated turbulent flow. *J. Fluid Mech.* **91**, 1.
- [5] Deardorff, J.W. and Willis, G.E., 1967, Investigation of turbulent convection between horizontal plates. *J. Fluid Mech.* **28**, 675.
- [6] Deardorff, J.W., 1973, The use of subgrid transport equations in a three-dimensional model of atmospheric turbulence. *J. Fluid Engineering* **95**, 429.
- [7] Eidson, T.M., 1985, Numerical simulation of the turbulent Rayleigh-Benard problem using subgrid modeling. *J. Fluid Mech.* **158**, 145.
- [8] Eidson, T.M., Hussaini, M.Y. and Zang, T.A., 1986, Simulation of the turbulent Rayleigh-Benard problem using a spectral/finite difference technique. In *Proceeding of the EUROMECH Colloquium No. 199* (ed. U. Schumann and R.Friedrich), p. 188, Vieweg, Braunschweig.
- [9] Grotzbach, G., 1982, Direct numerical simulation of laminar and turbulent Benard convection. *J. Fluid Mech.* **119**, 145.
- [10] Lilly, D.K., 1967, The representation of small-scale turbulence in numerical simulation experiments. In *Proc. of the IBM Scientific Computer Symposium on Environmental Sciences*, IBM Form No. 320-1951, p. 195.
- [11] Piomelli, U., Zang, T.A., Speziale, C.G. and Hussaini, M.Y., 1989, On the large-eddy simulation of transition wall-bounded flows. *Phys. Fluids A* **2**, 257.
- [12] Tennekes, H. and Lumley, J.L., 1972, *A First Course in Turbulence*, M.I.T. Press, Cambridge, Mass.

- [13] Reynolds, W.C., 1989, The Potential and Limitations of Direct and Large Eddy Simulations. *Lecture Notes in Physics: Whither Turbulence? Turbulence at the Crossroads* 357, ed. J.L. Lumley, Springer-Verlag.
- [14] Rogallo, R.S. and Moin, P., 1984, Numerical simulation of turbulent flows. *Ann. Rev. Fl. Mech.* 16, 99.

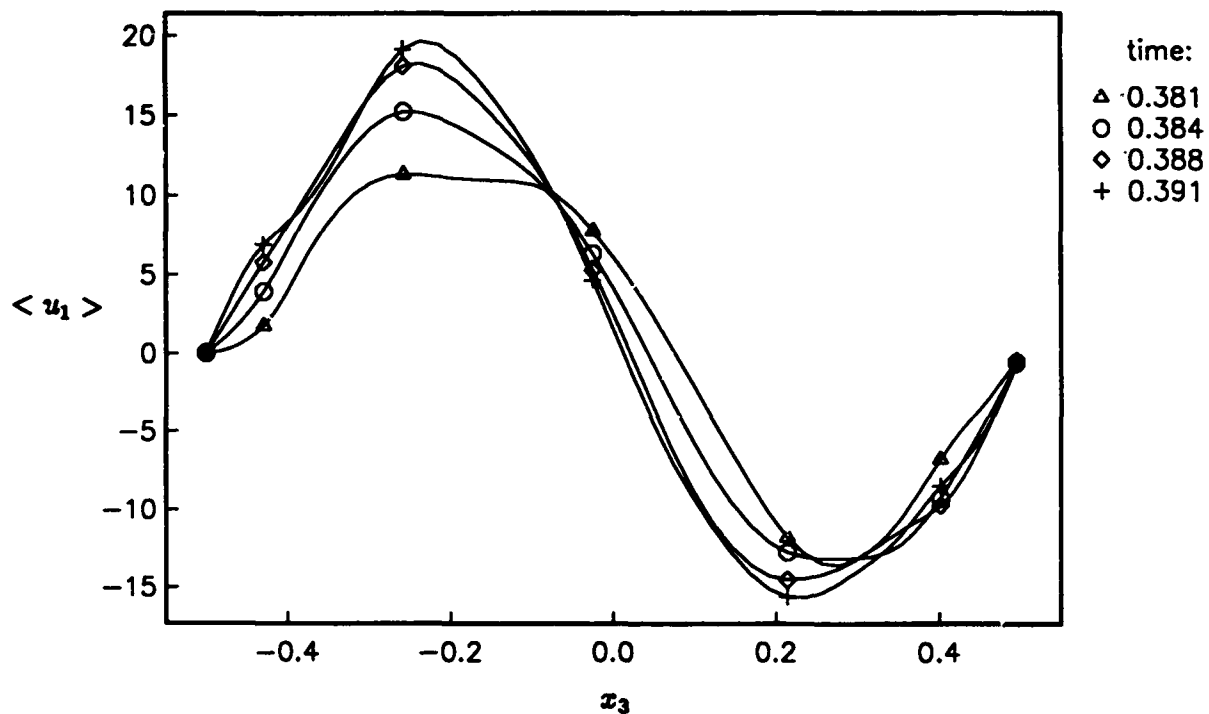


(a) Volume average of velocity

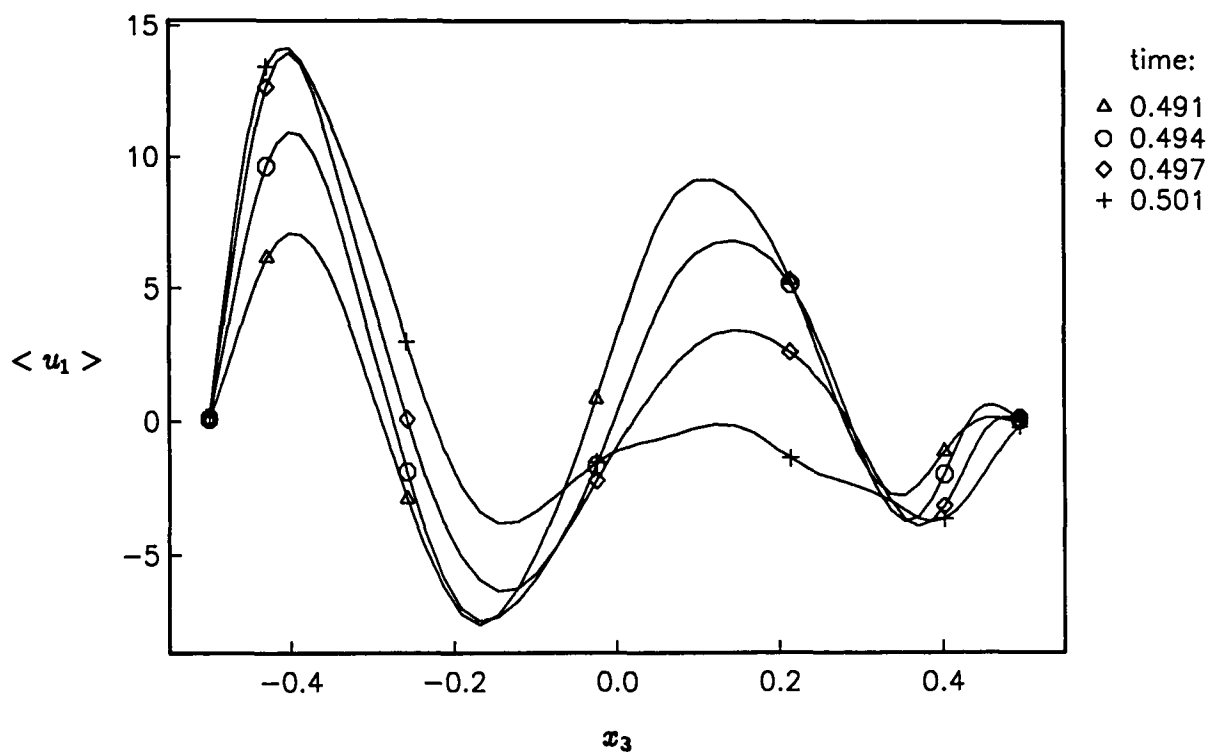


(b) Volume average of RMS velocity

Figure 1: Time evolution of the volume-averaged velocities during the simulation "steady state"

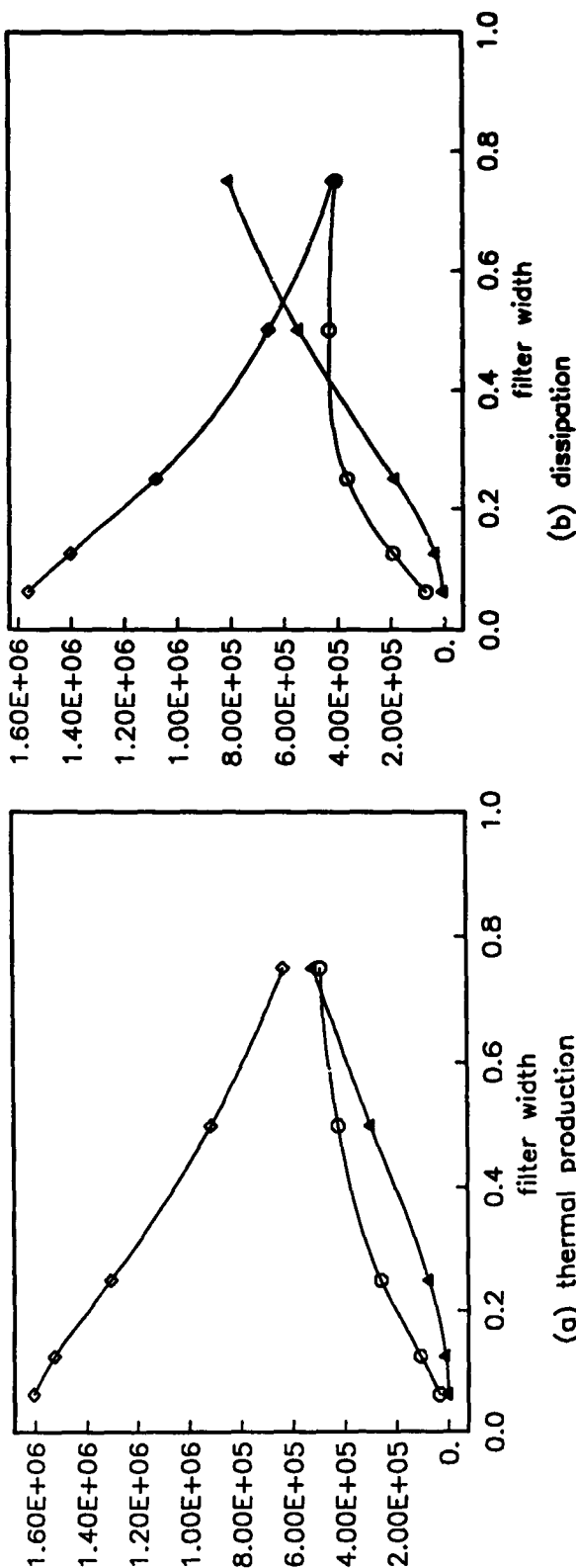


(a) First half of simulation

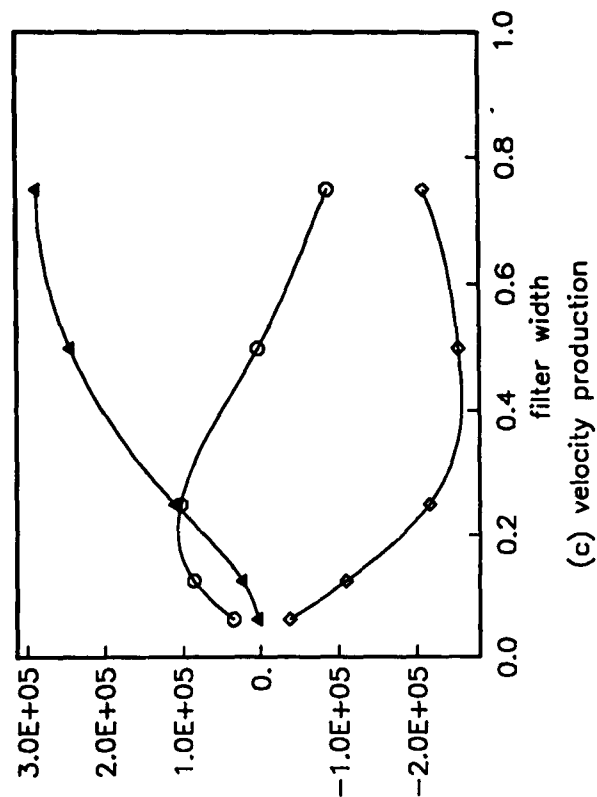


(b) Second half of simulation

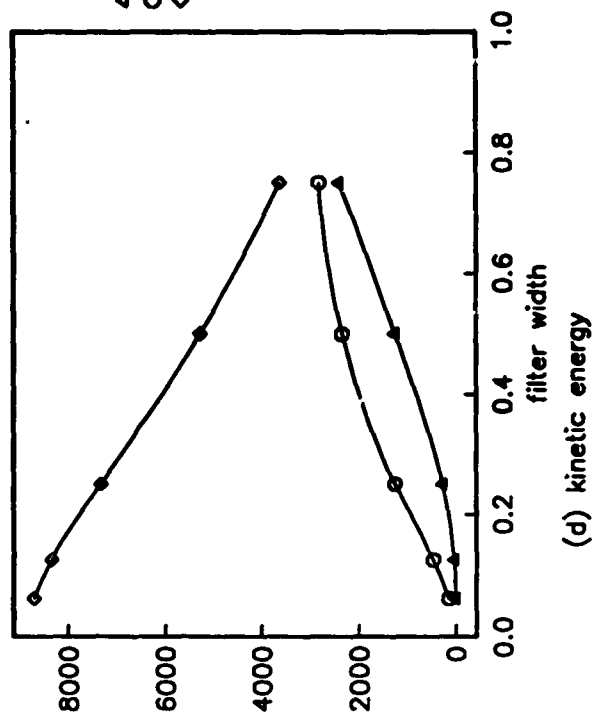
Figure 2: $\langle u_1 \rangle$ at selected time steps



(a) thermal production



(b) dissipation



(c) velocity production

Equation:
 ▲ Fluctuation
 ○ Cross
 ◇ Filtered

Figure 3: Volume-averaged terms in the set of filtered energy equations

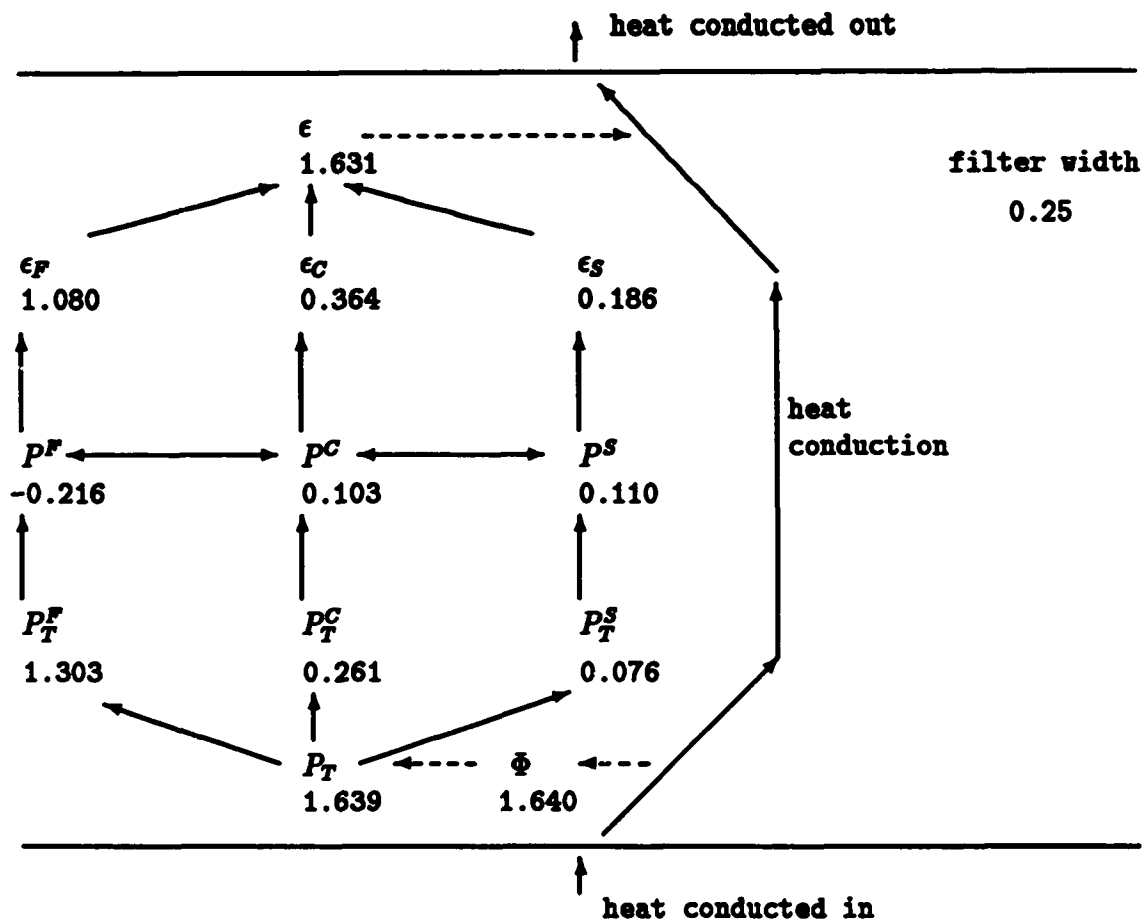


Figure 4: Volume-averaged energy flow diagram for filter width 0.25 . All data has been divided by 10^6 .

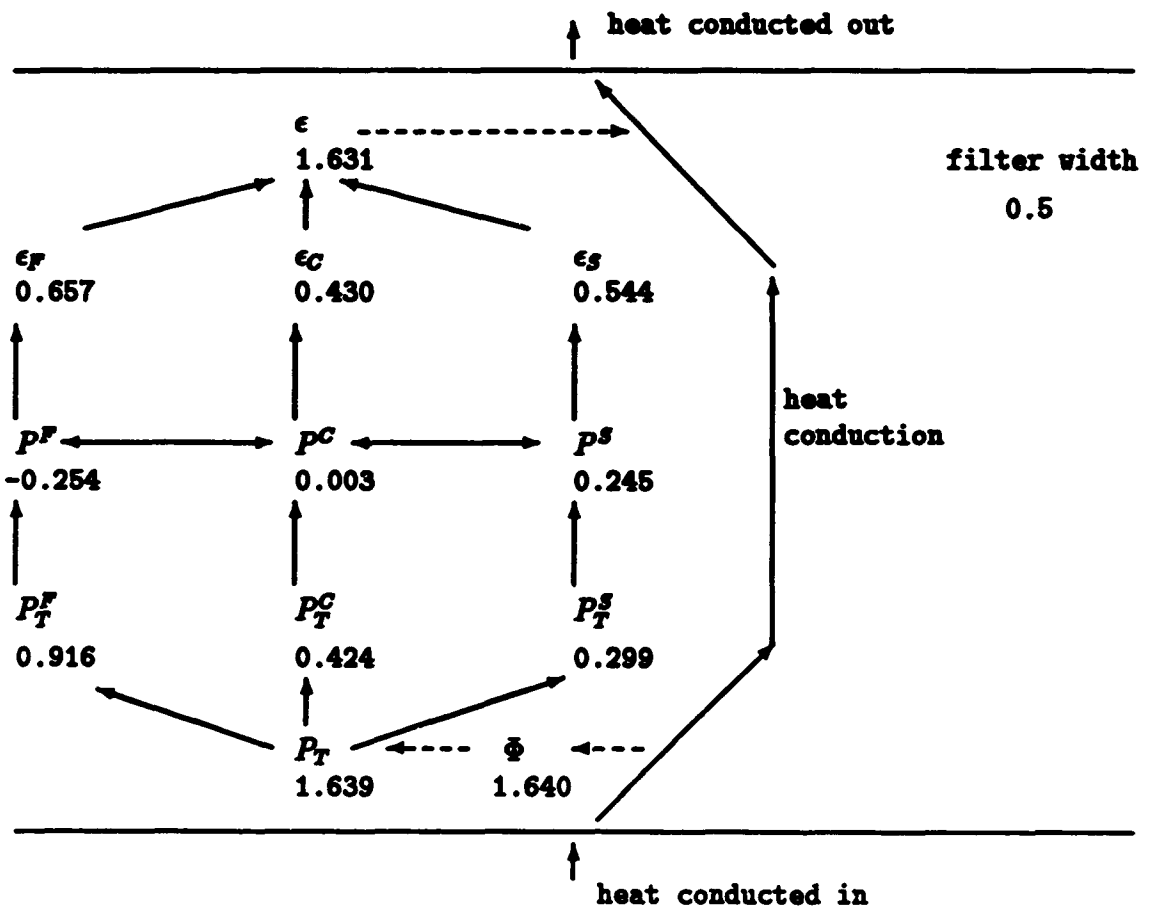
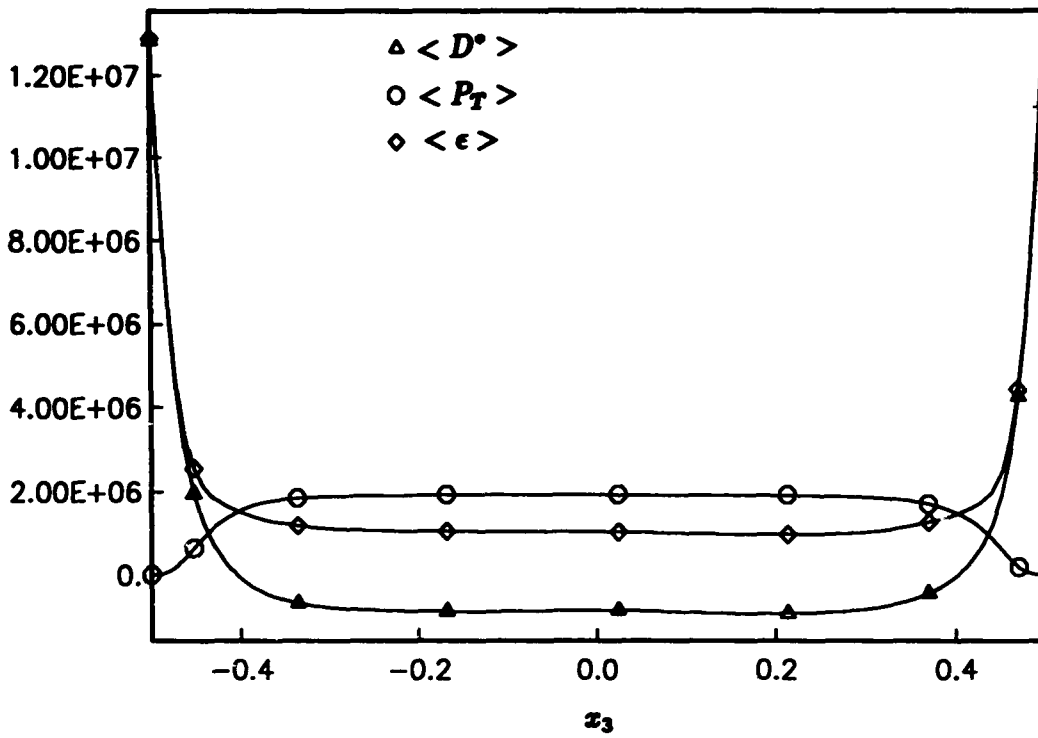
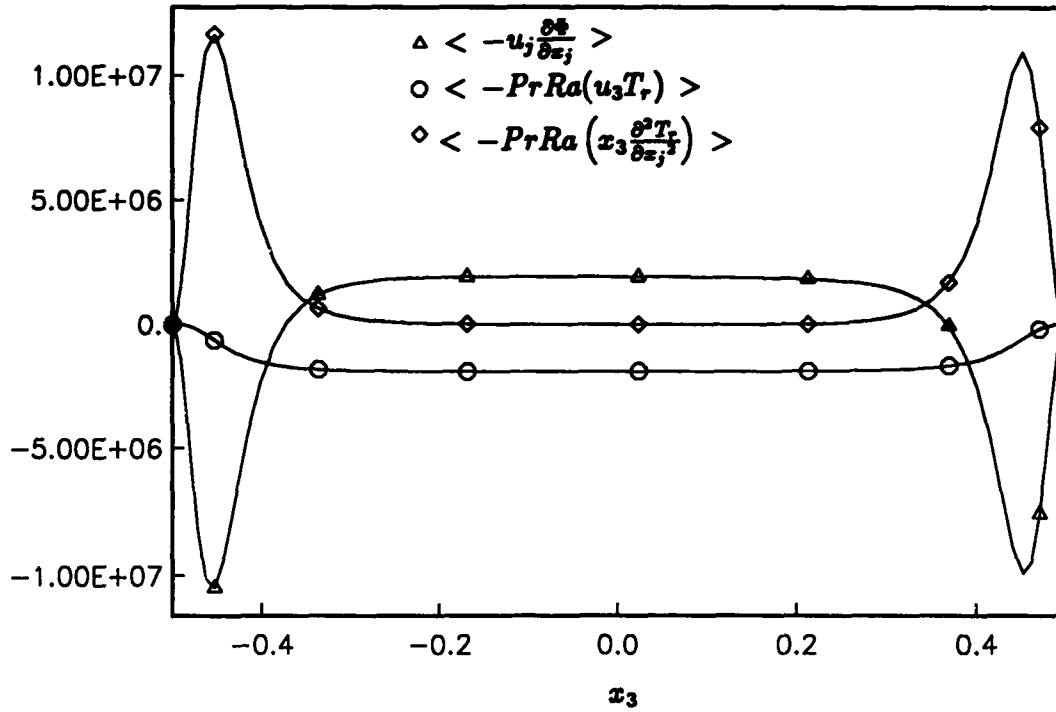


Figure 5: Volume-averaged energy flow diagram for filter width 0.50 . All data has been divided by 10^6 .



(a) kinetic energy equation



(b) potential energy equation

Figure 6: Horizontally-averaged terms of the total kinetic and potential energy equation

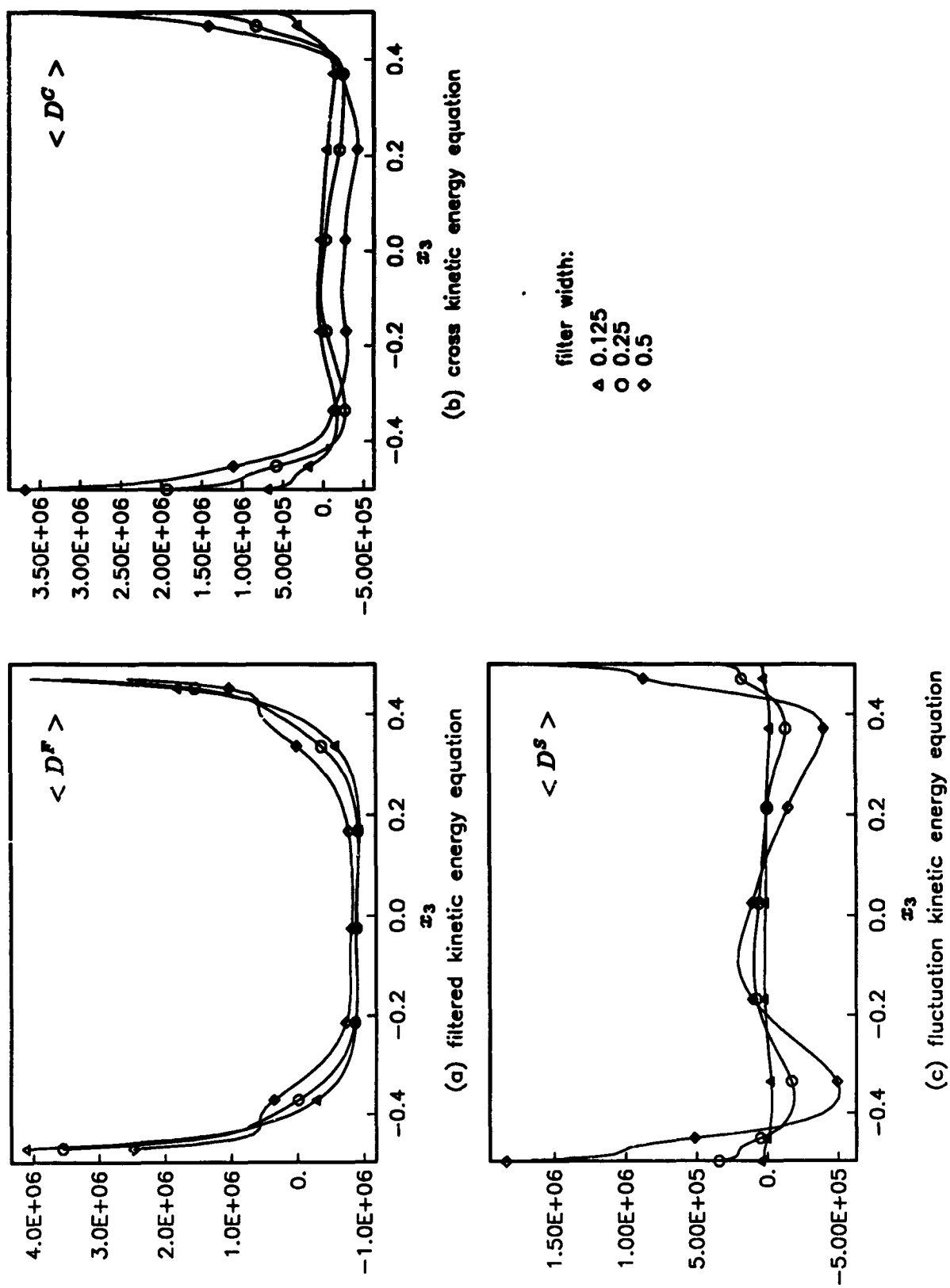
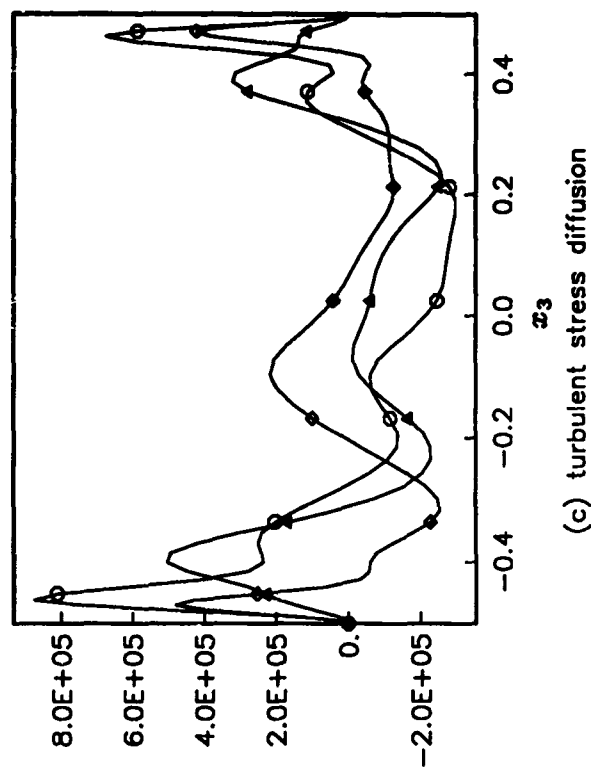
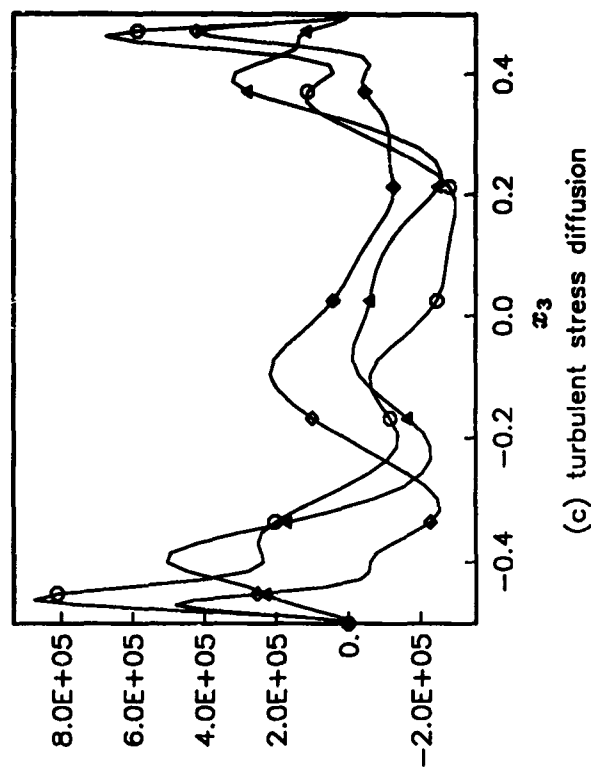
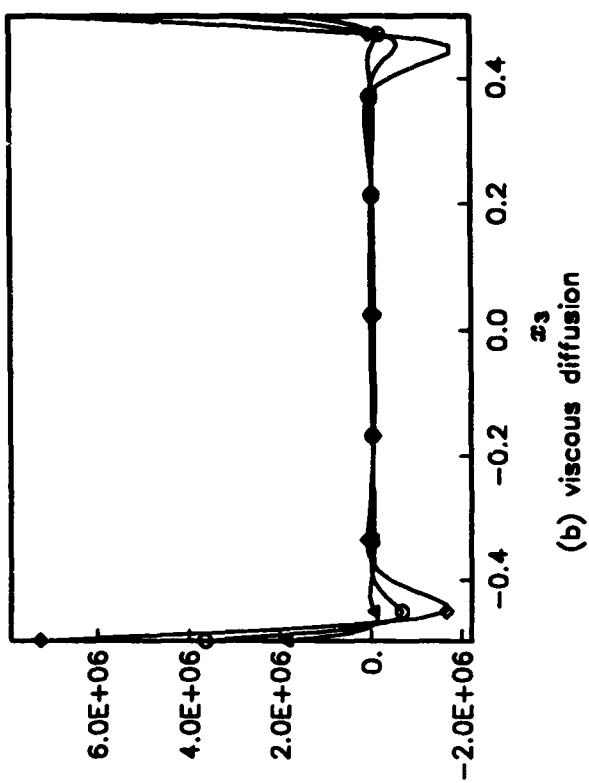


Figure 7: Horizontally-averaged diffusion term in the set of filtered kinetic energy equation



equation:
 Δ filtered
 \circ cross
 \diamond fluctuation

Figure 8: Horizontally-averaged components of the diffusion term for $\Delta_f = 0.5$

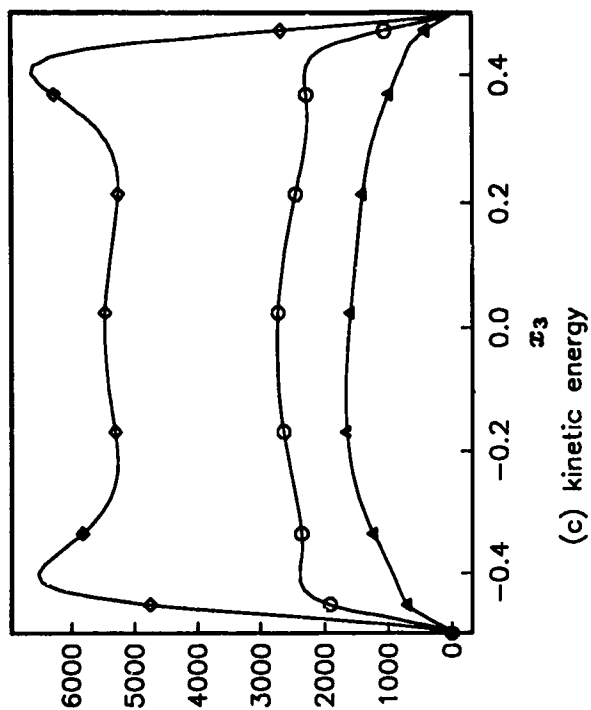
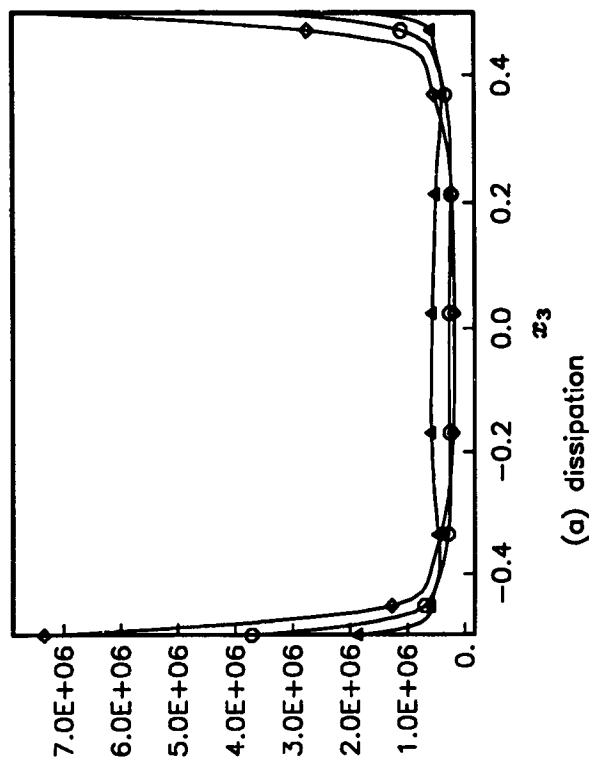
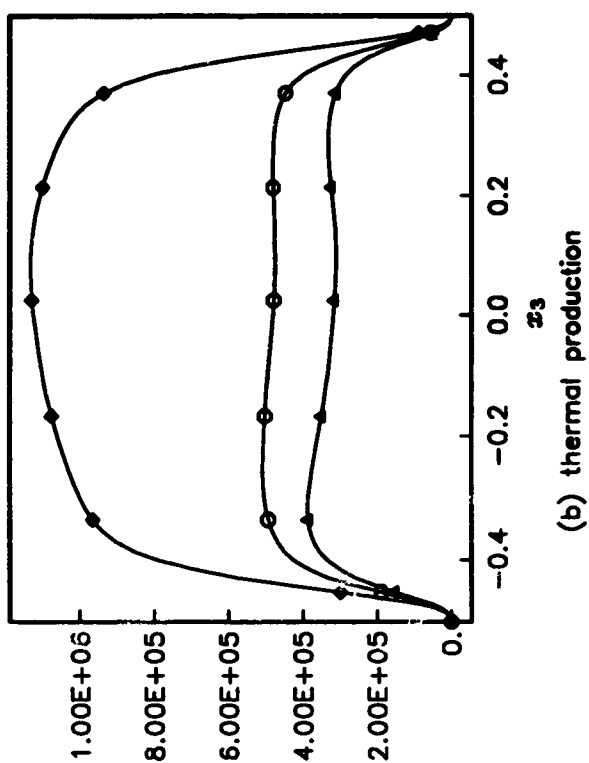
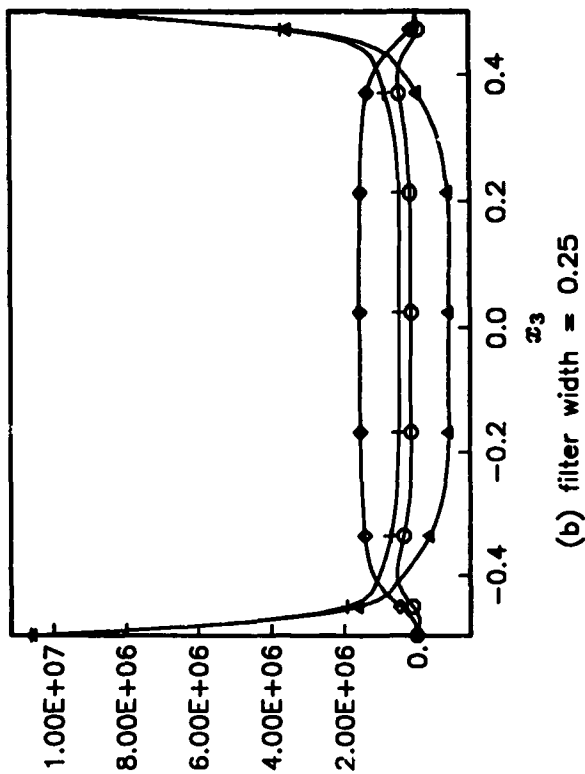


Figure 9: Horizontally-averaged terms in the set of filtered kinetic energy equations for $\Delta_f = 0.5$



Δ diffusion
 \circ velocity production
 \diamond thermal production
 $+$ dissipation

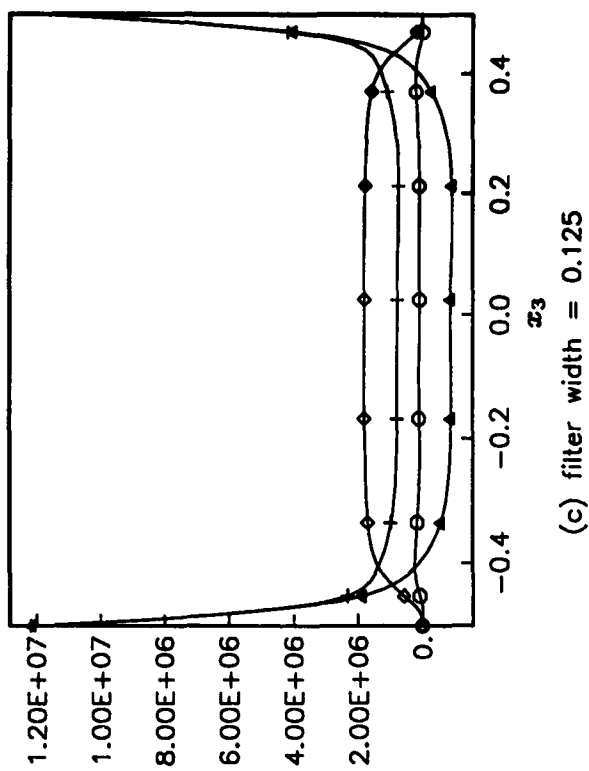
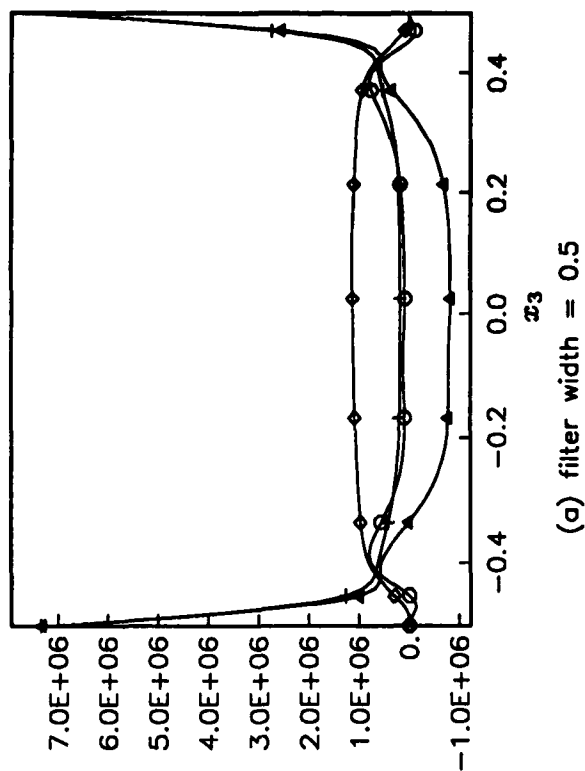
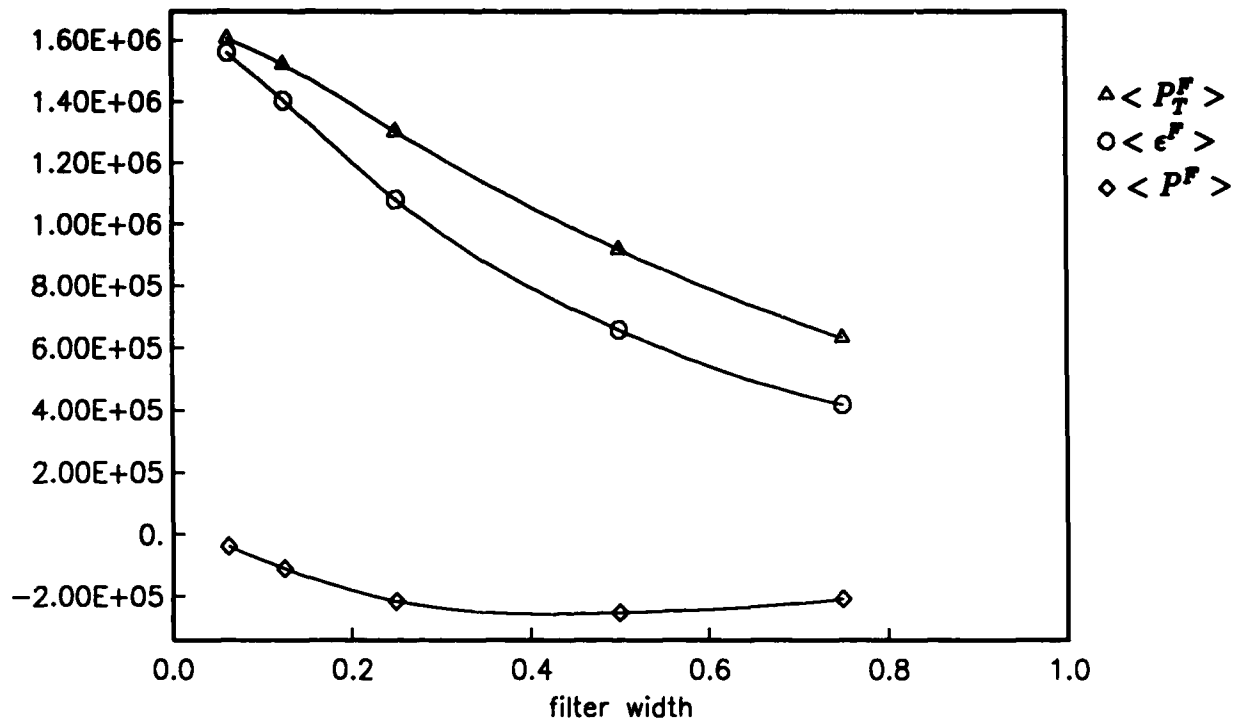
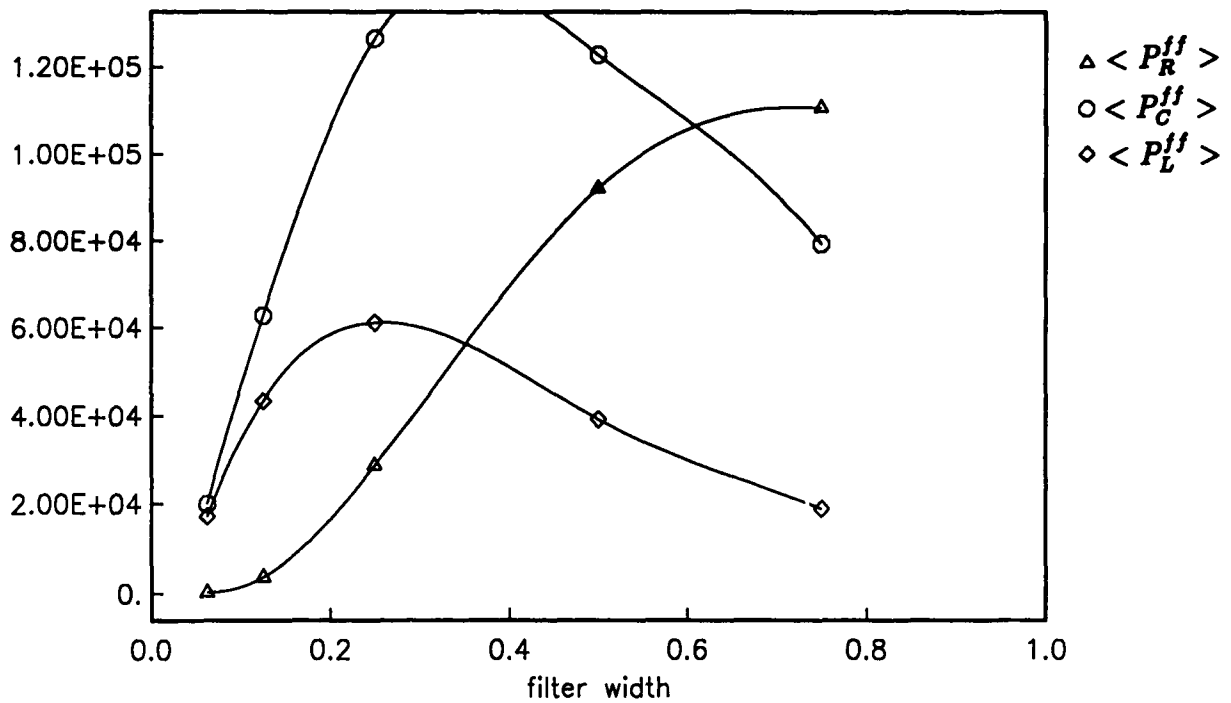


Figure 10: Horizontally-averaged terms in the filtered kinetic energy equation

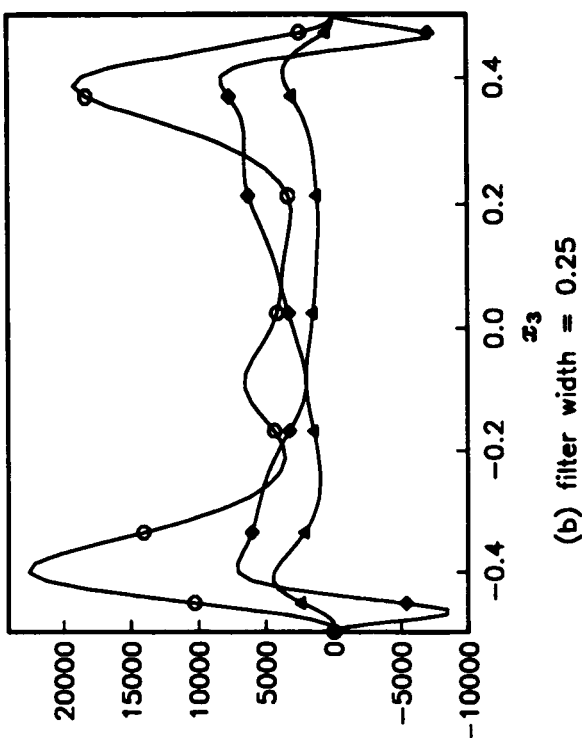


(a) Non-zero principal terms



(b) Components of velocity production

Figure 11: Volume-averaged terms in the filtered kinetic energy equation



$\triangle < P_R^{II} >$
 $\circ < P_C^{II} >$
 $\diamond < P_L^{II} >$

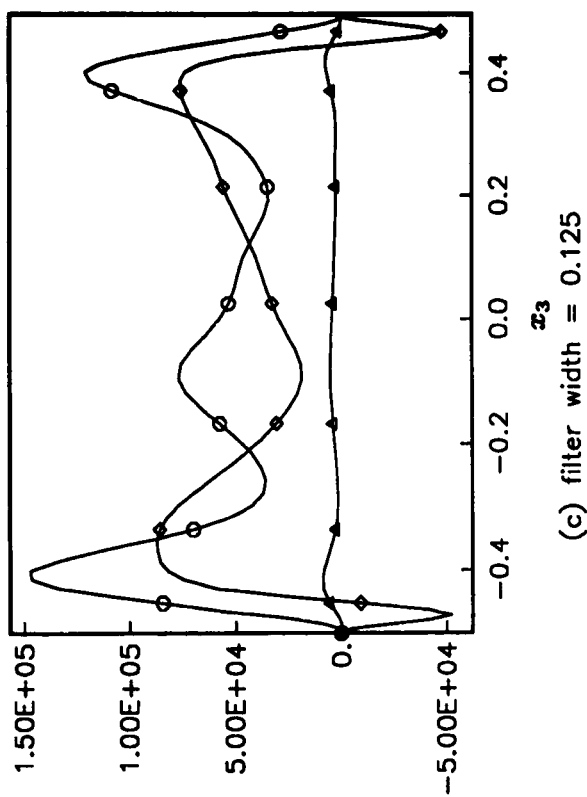
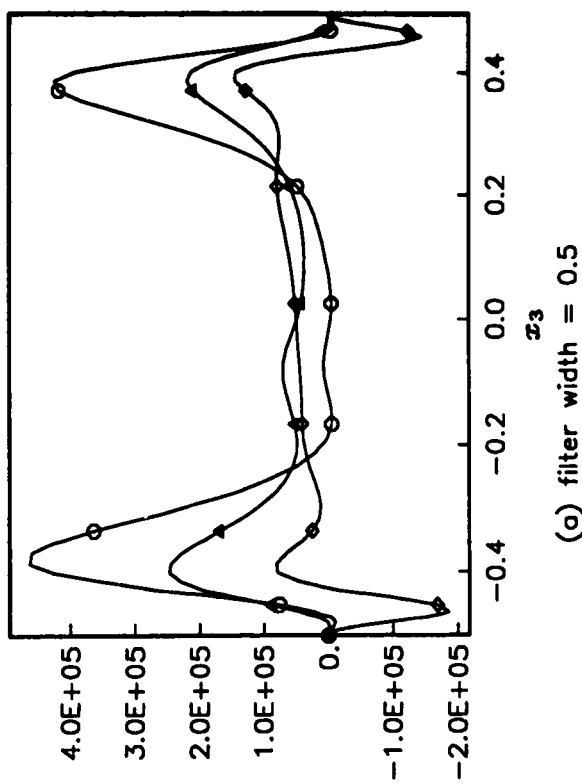
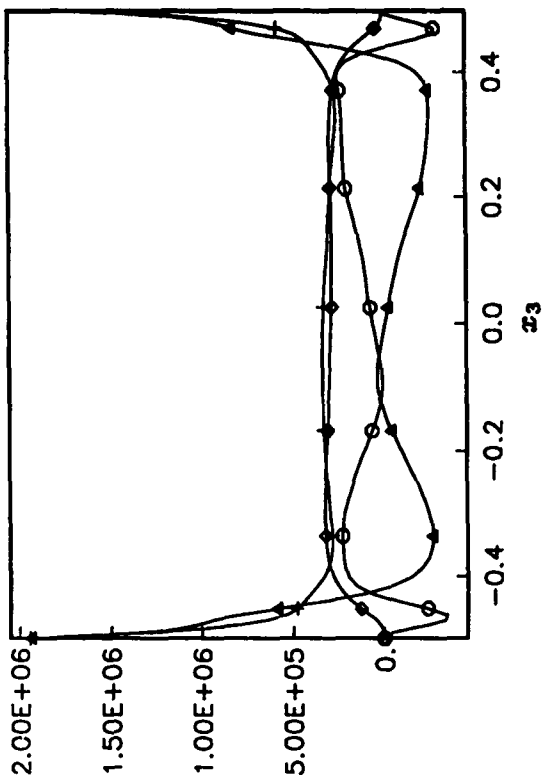


Figure 12: Horizontally-averaged components of the velocity production term in the filtered kinetic energy equation



Δ diffusion
 \circ velocity production
 \diamond thermal production
 $+$ dissipation

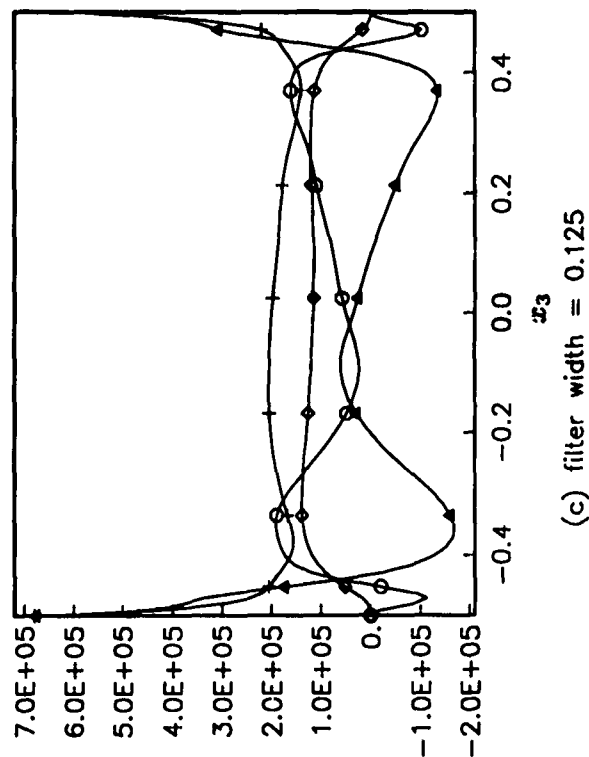
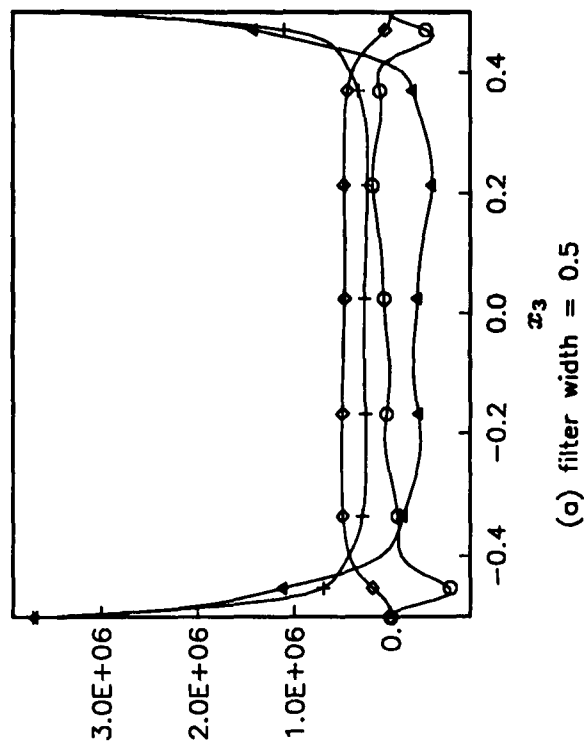
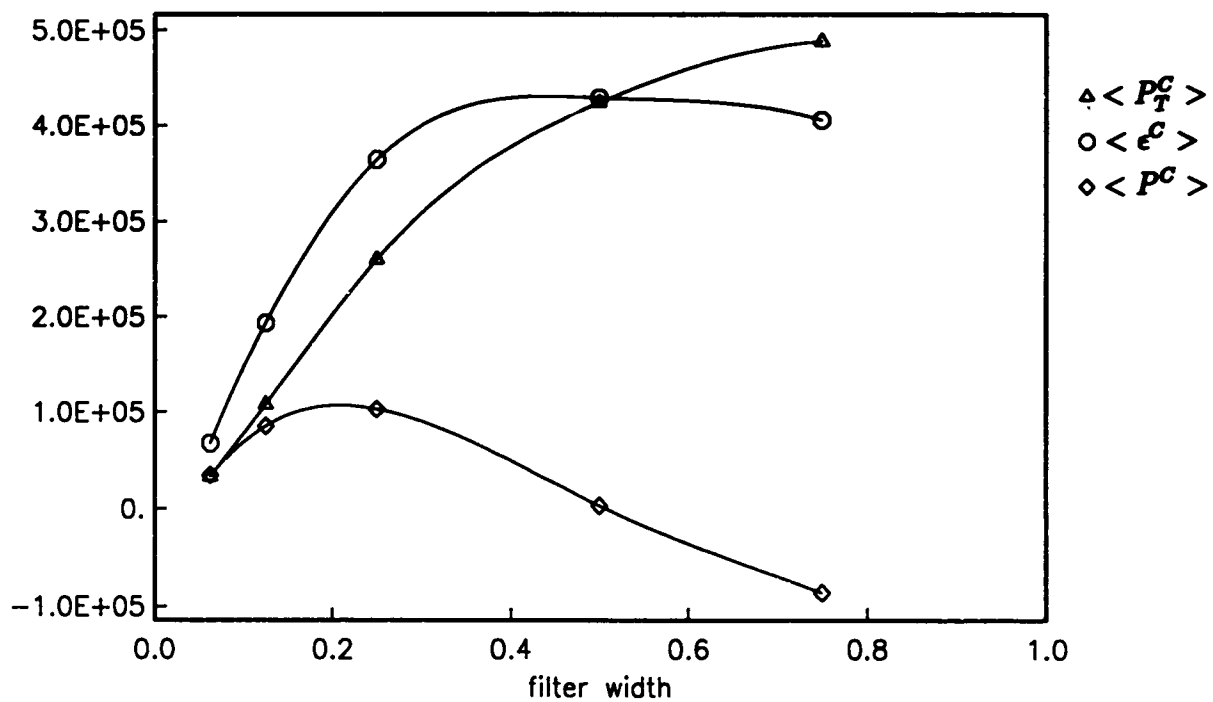
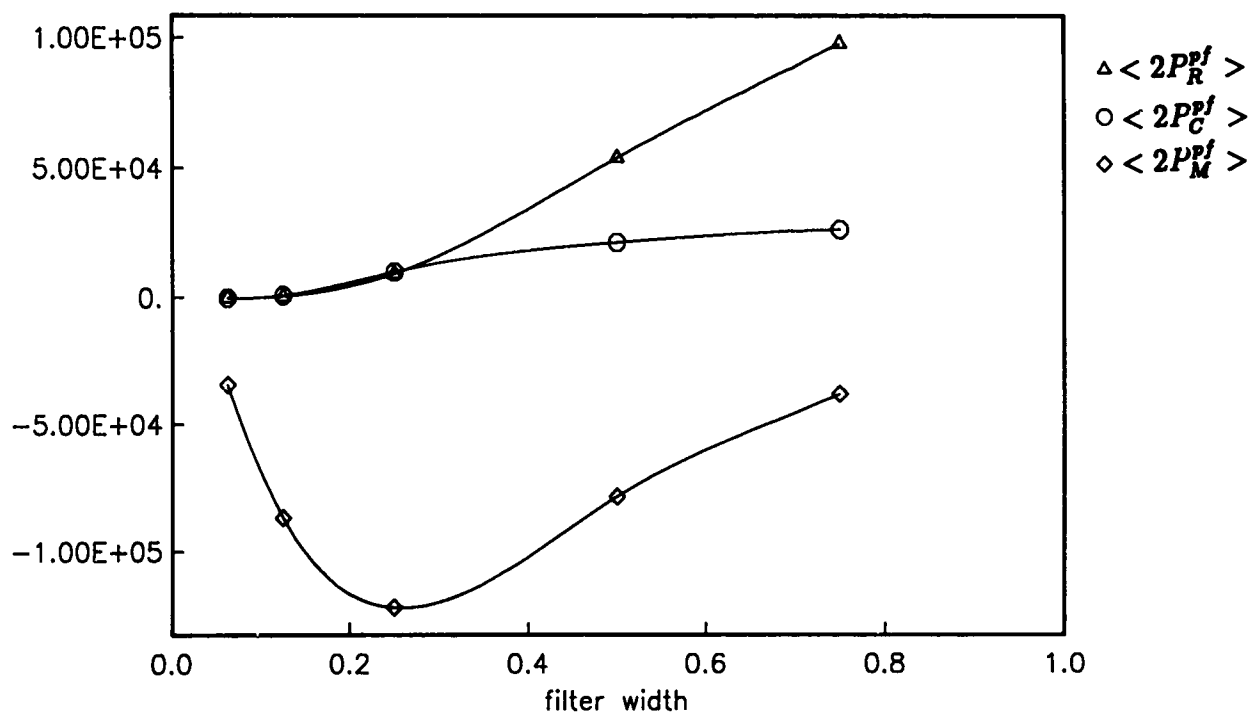


Figure 13: Horizontally-averaged terms in the cross kinetic energy equation

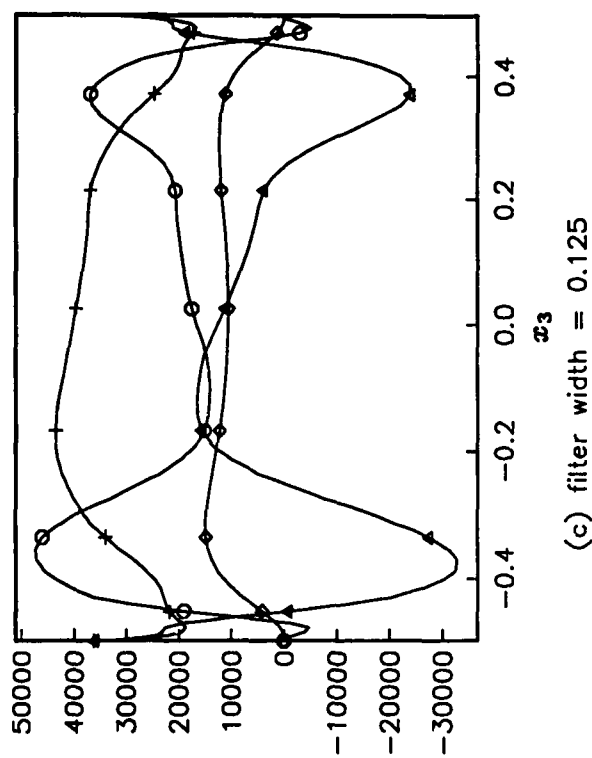
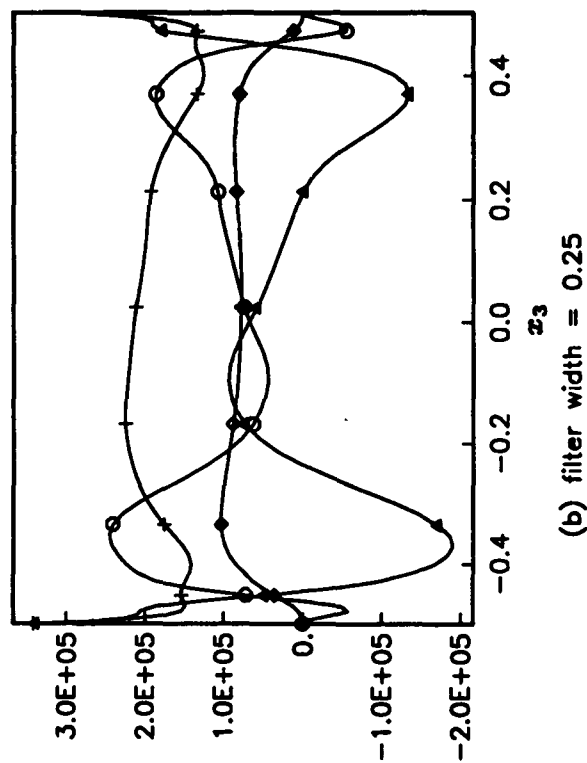
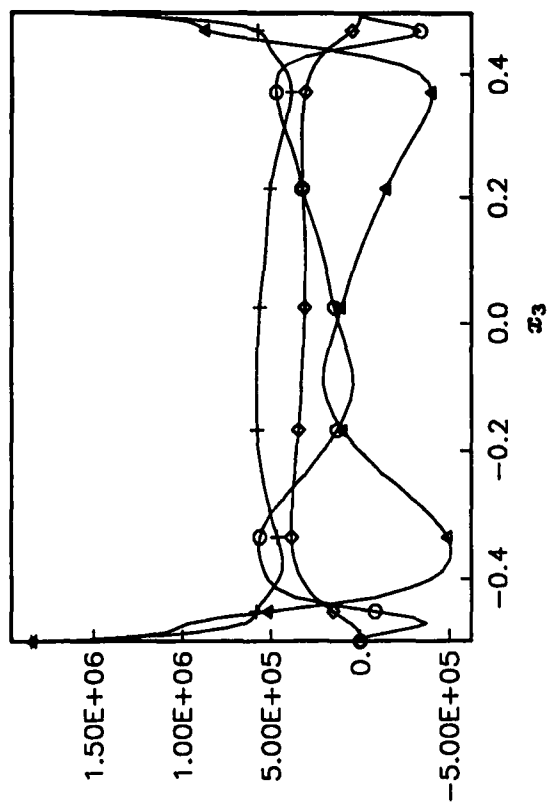


(a) Non-zero principal terms



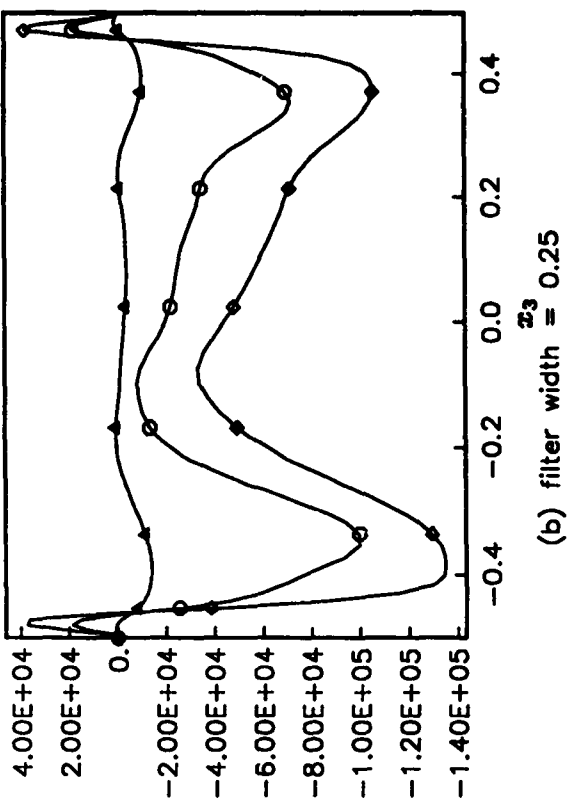
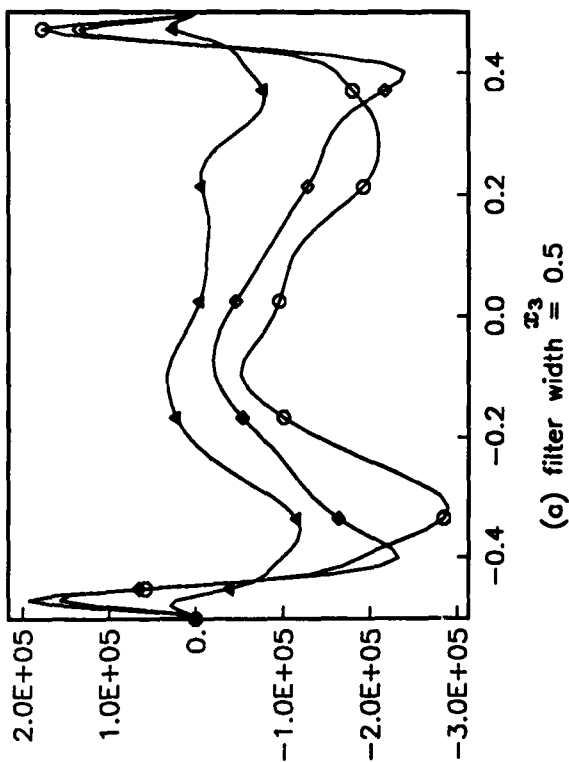
(b) Components of velocity production

Figure 14: Volume-averaged terms in the cross kinetic energy equation



Δ diffusion
 \circ velocity production
 \diamond thermal production
 $+$ dissipation

Figure 15: Horizontally-averaged terms in the fluctuation kinetic energy equation



$$\begin{aligned} \triangle & \langle P_R^{\mathcal{F}} \rangle > - \langle P_R^{\mathcal{F}} \rangle \\ \circ & \langle P_C^{\mathcal{F}} \rangle > - \langle P_C^{\mathcal{F}} \rangle \\ \diamond & \langle P_L^{\mathcal{F}} \rangle > - \langle P_L^{\mathcal{F}} \rangle \end{aligned}$$

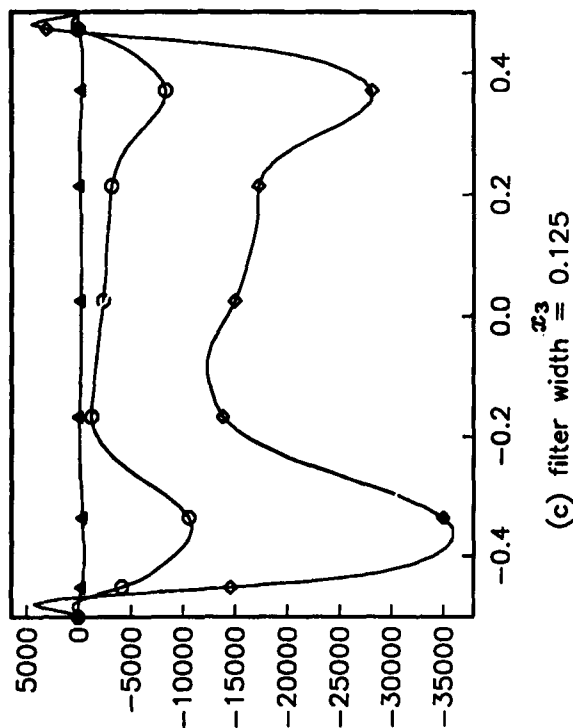
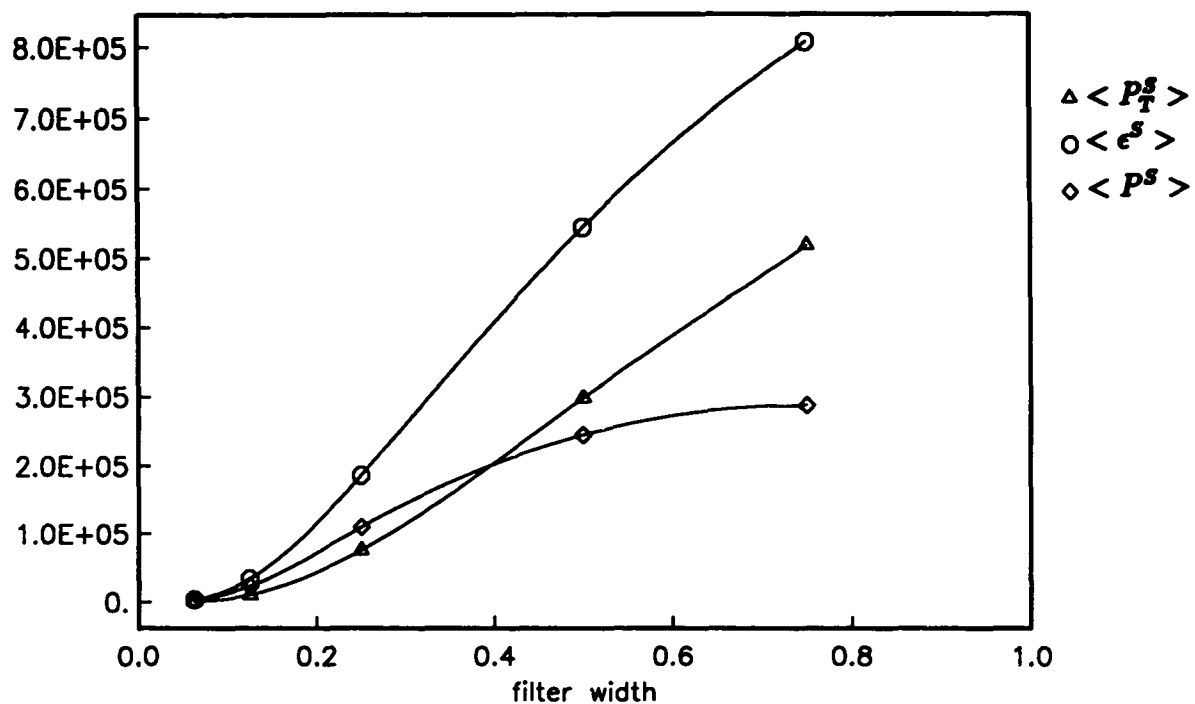
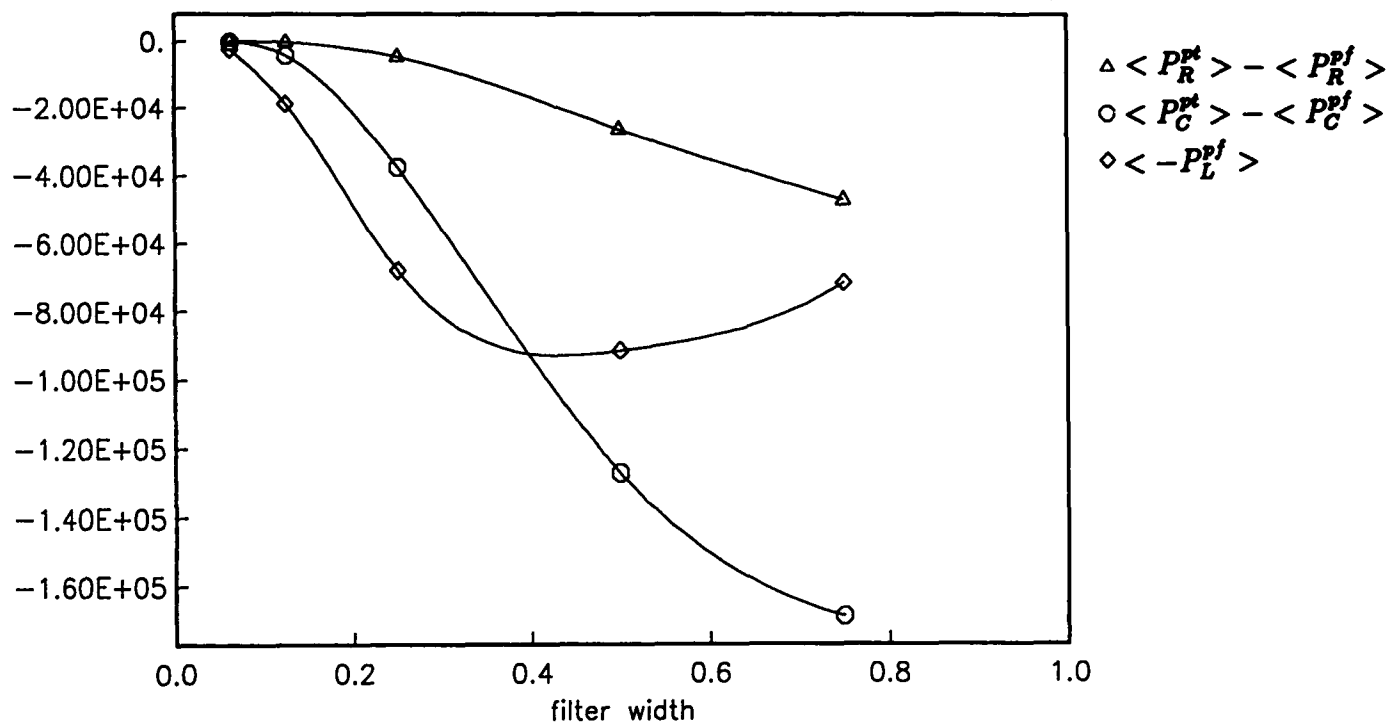


Figure 16: Horizontally-averaged components of the velocity production term in the fluctuation kinetic energy equation.



(a) Non-zero principal terms



(b) Components of velocity production

Figure 17: Volume-averaged terms in the fluctuation kinetic energy equation

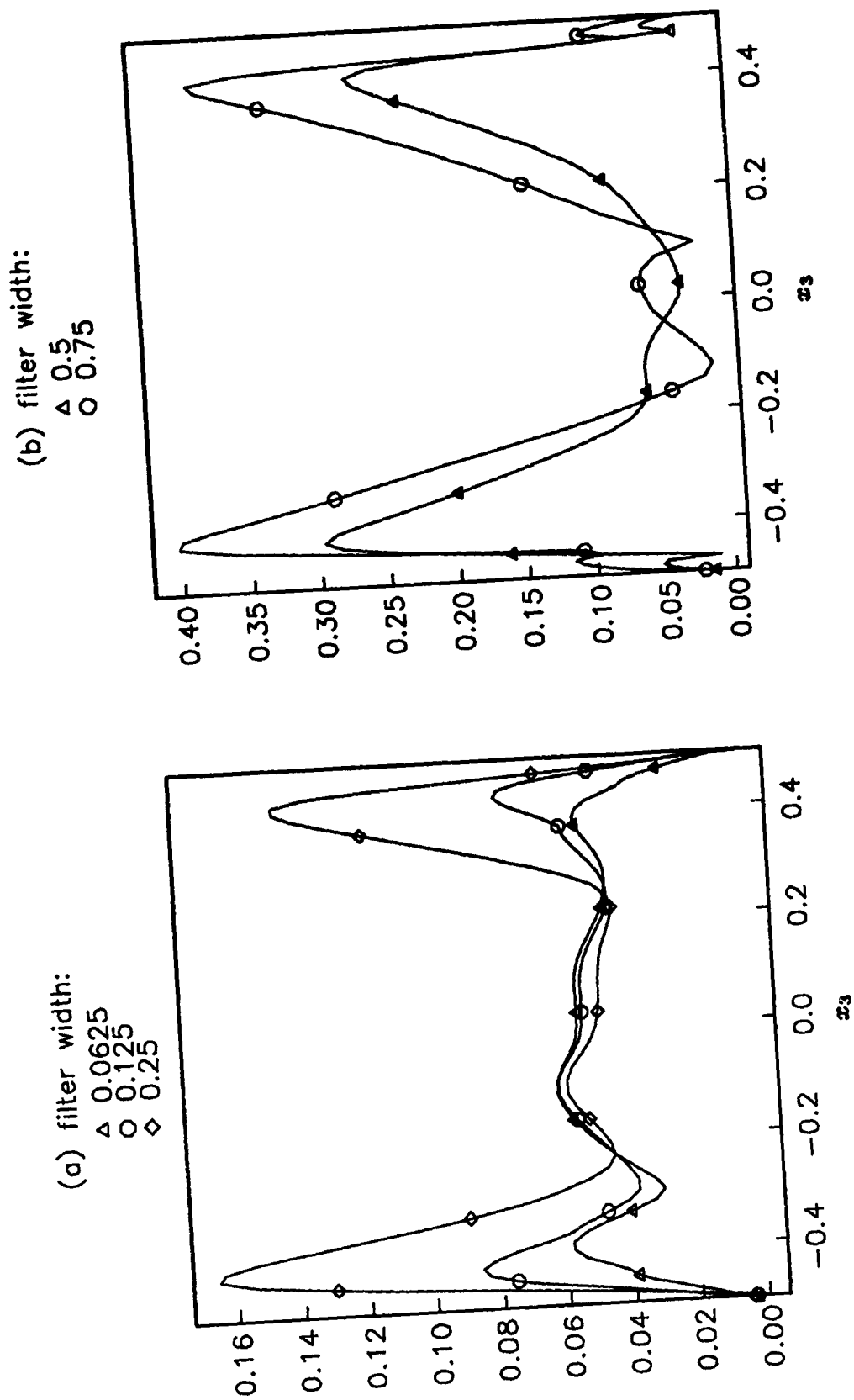


Figure 18: C_k versus x_3 for modified Smagorinsky model

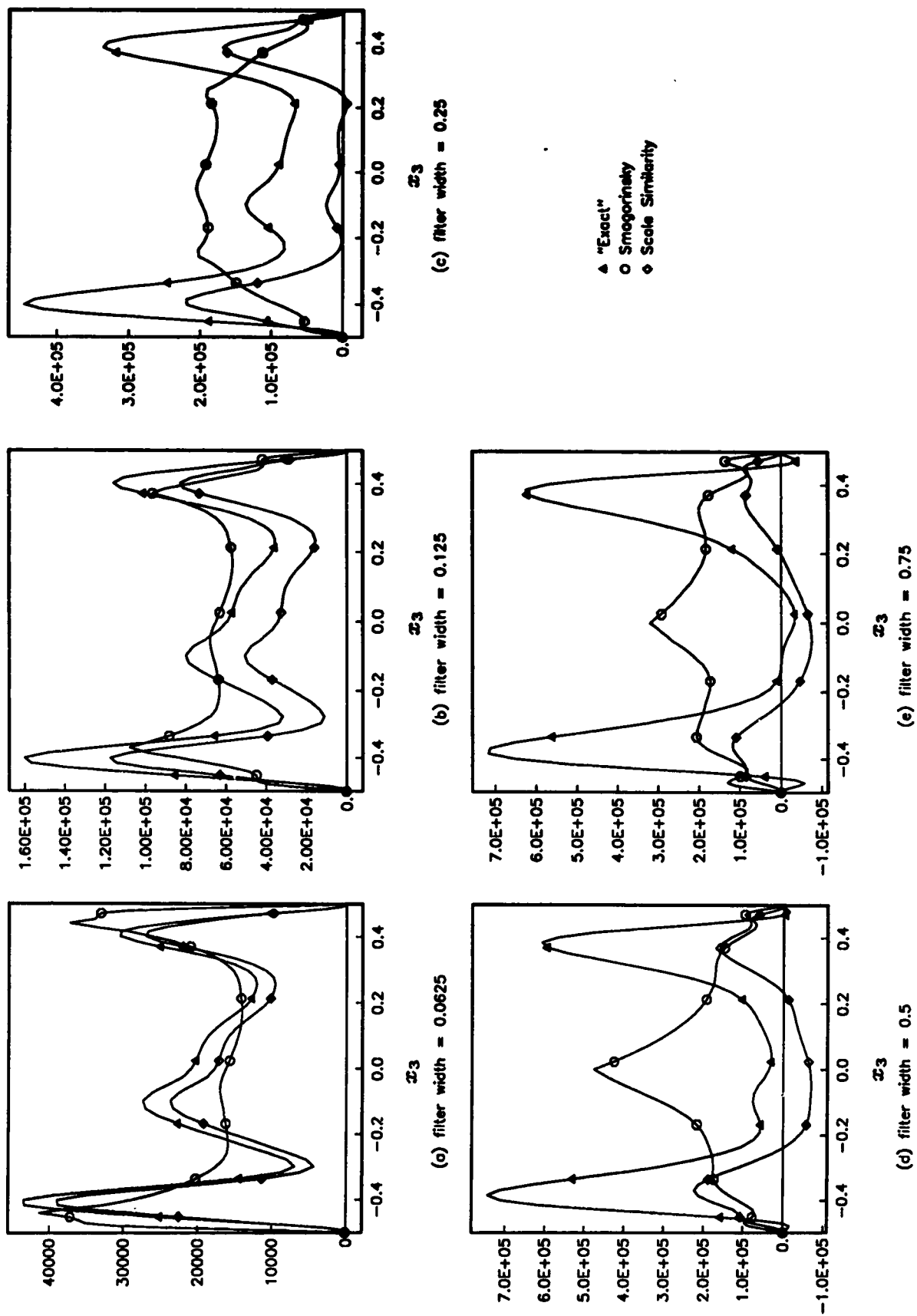


Figure 19: Horizontal average of P_{R+C}^{ff} - simulation and 2 models

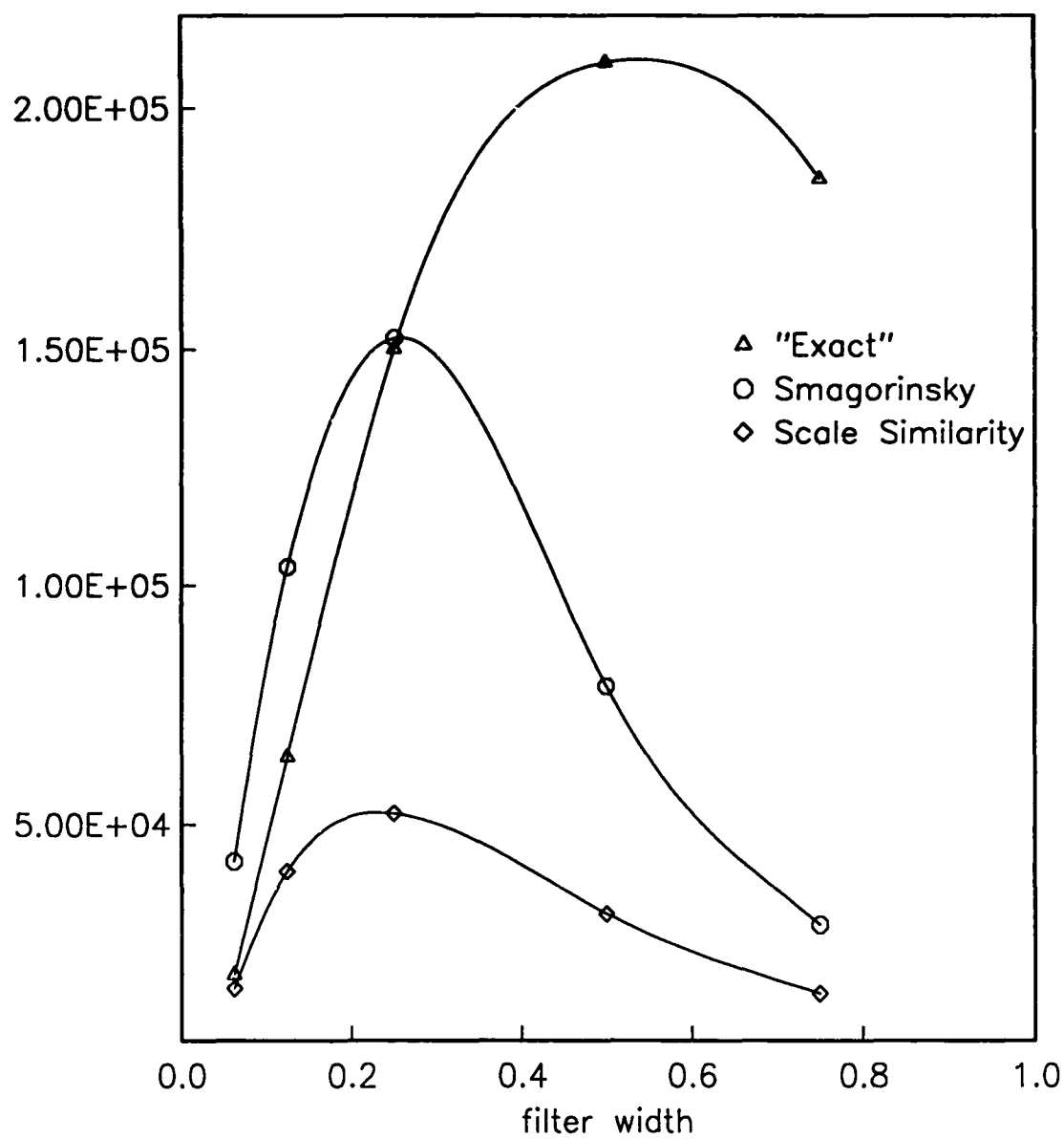


Figure 20: Volume average of P_{R+C}^{ff} - simulation and 2 models

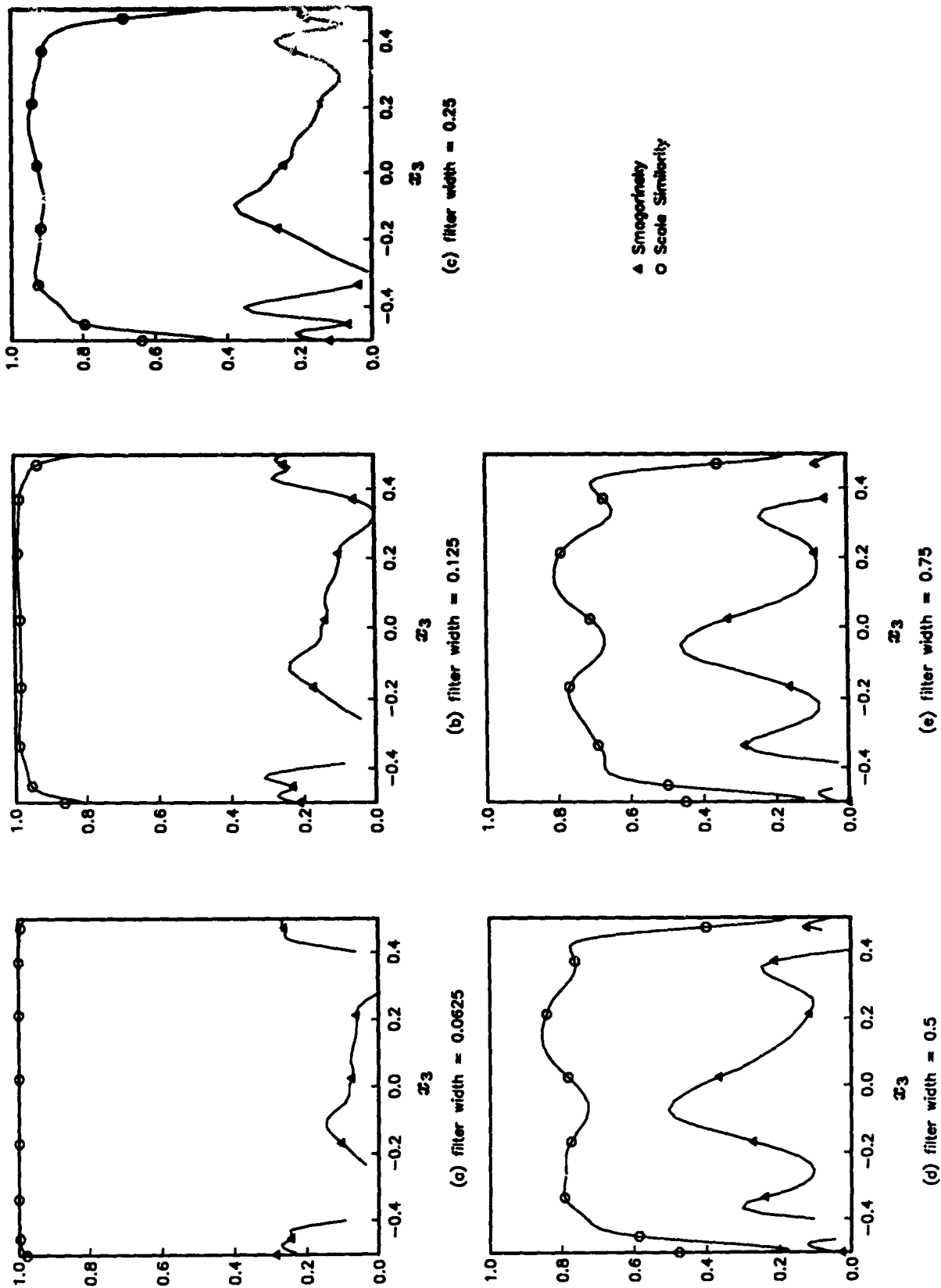


Figure 21: Correlation of 2 models with simulation results for P_{R+c}



Report Documentation Page

1. Report No. NASA CR-187488 ICASE Interim Report No. 15		2. Government Accession No.		3. Recipient's Catalog No.	
4. Title and Subtitle FILTERING ANALYSIS OF A DIRECT NUMERICAL SIMULATION OF THE TURBULENT RAYLEIGH-BENARD PROBLEM				5. Report Date December 1990	
				6. Performing Organization Code	
7. Author(s) T. M. Eidson T. A. Zang				8. Performing Organization Report No. Interim Report No. 15	
				10. Work Unit No. 505-90-21-01	
9. Performing Organization Name and Address Institute for Computer Applications in Science and Engineering Mail Stop 132C, NASA Langley Research Center Hampton, VA 23665-5225				11. Contract or Grant No. NAS1-18605	
				13. Type of Report and Period Covered Contractor Report	
12. Sponsoring Agency Name and Address National Aeronautics and Space Administration Langley Research Center Hampton, VA 23665-5225				14. Sponsoring Agency Code	
15. Supplementary Notes Langley Technical Monitor: Richard W. Barnwell Final Report					
16. Abstract <p>A filtering analysis of a turbulent flow has been developed which provides details of the path of the kinetic energy of the flow from its creation via thermal production to its dissipation. A low-pass spatial filter is used to split the velocity and the temperature field into a filtered component (composed mainly of scales larger than a specific size, nominally the filter width) and a fluctuation component (scales smaller than a specific size). Variables derived from these fields can fall into one of the above two ranges or be composed of a mixture of scales dominated by scales near the specific size. The filter is used to split the kinetic energy equation into three equations corresponding to the three scale ranges described above.</p> <p>The data from a direct simulation of the Rayleigh-Benard problem for conditions where the flow is turbulent is used to calculate the individual terms in the three kinetic energy equations. This is done for a range of filter widths. These results are used to study the spatial location and the scale range of the thermal energy production, the cascading of kinetic energy, the diffusion of kinetic energy and the energy dissipation. These results are used also to evaluate two subgrid models typically used in large-eddy simulations of turbulence. Subgrid models attempt to model the energy below the filter width that is removed by a low-pass filter.</p>					
17. Key Words (Suggested by Author(s)) turbulence, filtering analysis, subgrid modeling, Rayleigh-Benard flow			18. Distribution Statement 34 - Fluid Mechanics and Heat Transfer 64 - Numerical Analysis Unclassified - Unlimited		
19. Security Classif. (of this report) Unclassified		20. Security Classif. (of this page) Unclassified		21. No. of pages 50	22. Price A03